

**Modelling the impact of polymer swelling on
production, reactor behaviour and polymer particle size
distribution of polyethylene**

Rita Ferreira Alves

Thesis to obtain the Master of Science Degree in

Chemical Engineering

Supervisors: Prof. Dr. Maria Rosário Gomes Ribeiro (IST)
Dr. Timothy F. L. McKenna (CPE/LCPP)
Prof. Dr. Carla Isabel Costa Pinheiro

Examination Committee

Chairperson: Prof. Dr. Carlos Manuel Faria de Barros Henriques
Supervisor: Prof. Dr. Maria Rosário Gomes Ribeiro (IST)
Members of the Committee: Prof. Dr. João Miguel Silva

June 2016

This page was intentionally left blank.

Acknowledgements

I would like to first express my gratitude to my supervisor in the Laboratory for the Chemistry and Processes of Polymerization (LCP), Dr. Timothy F.L. McKenna. Thank you for the amazing opportunity to work with you in Lyon, all the shared knowledge and the support you've given me.

I would also like to thank my supervisors in IST, Professor Maria Rosário and Professor Carla Pinheiro for their support and interest in this project.

A special thank you to Mr. Muhammad Ahsan Bashir, from LCP and Mr. Duarte Cecílio. You were both a crucial part of this work and it wouldn't be complete without your continuous input and ideas. To Mr. Bashir, a warm thank you for always being available for a short-notice five-minute meeting and for all the friendship in the six months I spent in Lyon.

On a more personal note, I'd like to thank Ms. Ana Rita, Ms. Monica Duarte, Mr. Renato Wong and Mr. Ricardo Marques. You were there from the beginning and helped me every step of the way. Your friendship truly is invaluable to me.

I'd also like to thank Mr. Jethro Bellman for the continuous support in the past few months. You've been a true friend and all your feedback was much appreciated.

Lastly, I would like to thank my family. My aunt, Ms. Ana Ferreira, my uncle, Dr. Pedro Montalvão and my cousin, Mr. Pedro Rodrigues. Your education, support and love is irreplaceable. To my mother, Ms. Maria João, there are no words to describe my gratitude. Your constant support, love and friendship modeled the person I am today. I could not have done this without you.

This page was intentionally left blank.

Abstract

The present work studies the impact of polyethylene swelling in a gas-phase fluidized bed reactor behavior and product particle size distribution. This study is carried out by adding an inert alkane to polyethylene production in gas-phase and dry mode.

The developed model estimates the polyethylene production and reactor's operating conditions, such as temperature and bed porosity in steady-state. Ethylene concentration in the active sites is estimated using the Sanchez-Lacombe EOS thermodynamic model

The model was validated through comparison with patent US 6864332 B2.

Results, show that the presence of an inert alkane increases reactor production, decreases reactor temperature and increases mean particle size. The bigger the alkane molecule size, the more noticeable the effects are.

Key Words: Polyethylene, Gas-phase, Dry mode, FBR modelling, Particle Size distribution, swelling.

Resumo

O trabalho aqui apresentado estuda o impacto de *swelling* de polietileno no funcionamento do reactor e na distribuição de tamanho de partículas do polímero. Este estudo é realizado adicionando um alcano inerte ao processo de produção de polietileno em fase gasosa e modo seco.

O modelo desenvolvido calcula a produção de polietileno e condições de operação do reactor, como temperatura e porosidade do leito, em estado estacionário. A concentração de etileno nos sítios activos é prevista pelo modelo termodinâmico de Sanche-Lacombe.

O modelo foi validado por comparação com a patente US 6864332 B2.

Os resultados mostram que incluir um alcano inerte aumenta a produção de polietileno, diminui a temperatura do reactor e aumenta o tamanho médio da partícula de polímero. Verifica-se ainda que quanto maior o tamanho da molécula de alcano adicionado, mais visível é o efeito do mesmo no sistema.

Palavras-chave: Polietileno, fase gasosa, Modo Seco, Modelação de FBR, Distribuição do tamanho da partícula, Inchaço do polímero.

This page was intentionally left blank.

Contents

Acknowledgements	iv
Abstract	viii
Resumo	x
List of Tables	xvi
List of Figures	xviii
Nomenclature	xx
Glossary	xxiii
0. Thesis Outline.....	1
1. Introduction.....	3
1.1. Properties of Polyethylene	3
1.2. Polyethylene Worldwide.....	5
1.3. Polyethylene Production	6
1.4. Motivation.....	7
2. Literature Review	9
2.1. General information on the Polyethylene Industrial Process.....	9
2.2. Gas-phase Reactors	10
2.2.1. Fluidized Bed Reactors for Polyethylene Production.....	12
2.2.2. Overview of the Induced Condensed Agents.....	15
2.2.3. Previous Models.....	17
2.3. Particle Size Distribution	18
2.3.1. Particle Fragmentation and Growth	18
2.3.2. Previous Models.....	19
3. Model Description.....	21
3.1. Model Equations	22
3.1.1. Mass Balances	22
3.1.2. Heat Balances	24
3.1.3. Bed Porosity and Pressure Drop.....	26
3.1.4. Particle Size Distribution	27
3.2. Model Implementation.....	28

4. Results.....	31
4.1. ICA effect on ethylene solubility and polymer density	31
4.2. Model Validation	33
4.3. Simulation I	35
4.4. Simulation II	38
4.5. Simulation III	39
4.6. Simulation IV	42
4.7. Sensitivity Analysis	44
4.7.1. Catalyst activity	45
4.7.2. Ethylene concentration in amorphous polymer phase	46
4.7.3. ICA partial pressure.....	47
4.7.4. Inlet Temperature	48
5. Conclusions	49
References	51
Appendix A	54
Appendix B	57
Appendix C	61
Appendix D	66

List of Tables

Table 1.1. Summary of the properties of PE categorized by density. All figures adapted from [4].	5
Table 2.1. Typical reactor conditions for gas-phase HDPE processes (adapted from [2][8][9]).	11
Table 2.2. FBR operating conditions for HDPE production [2][3][10].	14
Table 4.1. Properties of the solid phase, reaction parameters and reactor properties.	31
Table 4.2. Coefficients for the correlations of ethylene and ICA concentration on polymer phase (mol.m ⁻³) and polymer density (kg.m ⁻³).....	33
Table 4.3. Data used in the validation of the model (adapted from [39])	34
Table 4.4 – Comparison between the results presented in example 7C [39] and the simulation (Sim.) and the corresponding variation (Δ).	34
Table 4.5. Simulation I reactor parameters.	35
Table 4.6 - Simulation II reactor parameters.	38
Table 4.7 - Simulation III reactor parameters.	39
Table 4.8. Summary of the minimum fluidization, superficial and terminal velocities for the average particle size in the reactor. Values regarding simulation III.	41
Table 4.9. Average particle size for iso-butane and n-hexane at 80°C.	43
Table 4.10. Average particle size for propane and iso-butane at 70°C	44
Table 4.11. Sensitivity analysis results for the variation of kpT_{ref} (m ³ .mol ⁻¹ .s ⁻¹)	45
Table 4.12. Sensitivity analysis results for the variation of ethylene concentration in polymer phase (C_{EtP}) (mol.m ⁻³)	46
Table 4.13. Sensitivity analysis results for the variation of iso-butane partial pressure (P_{ICA}) (bar)	47
Table 4.14. Sensitivity analysis results for the variation of the inlet temperature (T_0) (K).....	48
Table A.0.1. Diluent/PE binary systems considered in this work.	55
Table B.1 - Component parameters for heat capacity calculations [37].	57
Table B.2 Coefficients for the viscosity (Pa.s) correlations.	58
Table B.3. Coefficients for the thermal conductivity (W.m ⁻¹ .K ⁻¹) correlations.....	58
Table C.1. Iso-butane solubility (C_{ICAP}) and effect on ethylene solubility (C_{EtP}) and amorphous polymer density (ρ_{PE}) at 80°C [44].	61
Table C.2. Iso-butane solubility (C_{ICAP}) and effect on ethylene solubility (C_{EtP}) and amorphous polymer density (ρ_{PE}) at 70°C [44].	61
Table C. 3. Propane solubility (C_{ICAP}) and effect on ethylene solubility (C_{EtP}) and amorphous polymer density (ρ_{PE}) at 70°C [43].	62
Table C.4. n-Hexane solubility (C_{ICAP}) and effect on ethylene solubility (C_{EtP}) and amorphous polymer density (ρ_{PE}) at 80°C	62
Table C.5. Results for propane at 70°C simulation I.	63
Table C.6. Results for iso-butane at 70°C simulation I and II.	63
Table C.7. Results for iso-butane at 80°C simulation II.	64

Table C.8 . Results for simulation III with propane at 74°C and constant production rate of 15,8 ton/h.....	64
Table C.9. Results for simulation III with iso-butane at 74°C and constant production rate of 15,8 ton/h.....	65

List of Figures

Figure 1.1. Polyethylene chemical structure. Adapted from [1].	3
Figure 1.2. Main downstream processes/applications of HDPE in 2007. Adapted from [4].	4
Figure 1.3. Main downstream processes/applications of LDPE (right) and LLDPE (left) in 2007. Adapted from [4].	4
Figure 1.4 – Demand for total polymer in 2012. Adapted from [5].	6
Figure 1.5 – Growth of Polyethylene's demand and future prospects. Adapted from [5].	6
Figure 2.1. Schematic representation of the a polyolefin production unit (adapted from [2]).	9
Figure 2.2. Unipol Process for PE production (adapted from [2])	10
Figure 2.3. Innovene G process from INEOS (adapted from [2]).	12
Figure 2.4 - Diagram of a fluidized bed reactor for PE production. Adapted from [2].	13
Figure 2.5 - Diagram of feed, recycle and cooling of the gas in an FBR (adapted from [2]).	15
Figure 2.6. Particle growth evolution. Adapted from [2].	18
Figure 3.1 Bed porosity vs Fluid superficial velocity (adapted from [20][36])	26
Figure 3.2. Main iterative cycle flowchart.	30
Figure 4.1 ICA effect on the concentration of ethylene in the polymer phase at 70° C and 80° C obtained from the SL-EoS in ternary (ethylene(1)/ICA(2)/PE(1)) systems	32
Figure 4.2. ICA effect on polymer density at 70°C and 80°C obtained from the SL-EoS in ternary (ethylene(1)/ICA(2)/PE(1)) systems.	33
Figure 4.3. Effect of ICA on reactor bulk and solids temperature for simulation I.	35
Figure 4.4. Effect of ICA on: (a) PE Production rate and (b) Ethylene per pass conversion. Values regarding simulation I.	36
Figure 4.5. Effect of ICA on polymer PSD for simulation I.	37
Figure 4.6. Effect of ICA on reactor pressure drop for simulation I.	37
Figure 4.7. Effect of ICA on reactor temperature for simulation II.	38
Figure 4.8. Effect of ICA on: (a) PE Production rate and (b) productivity. Values regarding simulation II.	39
Figure 4.9. Effect of ICA on: (a) Catalyst inlet flowrate and (b) gas inlet flowrate. Values regarding simulation III.	40
Figure 4.10. Effect of ICA on: (a) Productivity and (b) ethylene per pass conversion. Values regarding simulation III.	40
Figure 4.11. Effect of ICA on: (a) Superficial velocity and (b) bed porosity. Values regarding simulation III.	41
Figure 4.12. Effect of the ICA on polymer PDS for simulation III.	41
Figure 4.13. Effect of ICA on the polymer PSD at 80°C.	42
Figure 4.14. Effect of ICA on polymer PSD at 80°C (zoomed).	42
Figure 4.15. Effect of ICA on polymer PSD at 70°C.	43
Figure 4.16. Effect of ICA on polymer PSD at 70°C (zoomed).	43
Figure 4.17. Effect of temperature in polymer PDS for iso-butane (partial pressure 4 bar).	44

Figure A.1. Schematic representation of: (1) ethylene/polyethylene binary system and (2) ethylene/n-hexane/polyethylene ternary system at different magnifications. Adapted from [40].54

Figure A.2. Solubility of iso-butane, ethylene and their mixtures in LLDPE at 74°C. Fitting of the SL-EoS to binary experimental solubility data of iso-butane(1)/LLDPE(2) and ethylene(1)/LLDPE(2) systems at 74°C is shown for comparison. Experimental solubility data of ethylene(1)/LLDPE(2) obtained from [15]. 56

Nomenclature

Greek Symbols

α – Combined kinetic parameter

Δ – Expresses variation

ρ – Density

ε – Bed porosity

τ – Residence time

μ – Viscosity

Roman Symbols

A_p – Heat transfer area

Ar – Archimedes Number $\left(\frac{d_p^3 \cdot g \cdot \rho_{gas} \cdot (\rho_s - \rho_{gas})}{\mu^2} \right)$

A_s – Reactor cross section area

C – Concentration

Conversion – Ethylene per pass conversion

$\overline{C_p}$ – Component heat capacity at constant pressure

D, d – Diameter

E_a – Activation Energy

$F(D_p)$ – Numerical Particle Size Distribution

H – Enthalpy

h – Convective heat transfer coefficient

k_d – deactivation constant

k_p – kinetic rate constant

L – bed height

MW – Molecular weight

n_p – number of particles

P – Pressure

Productivity – Catalyst Productivity

Q – Component mass flowrate

R – Perfect Gas Constant

R_p – Rate of polymerization

T – Temperature

t – Polymerization time

u – Superficial velocity

V – Volume

Subscripts

bed, b – Refers to the catalyst/polymer bed

c – Refers to the catalyst or catalyst particle

d – Dissolved in the polymer phase

Et – Ethylene

gas – Refers to the gas-phase

ICA – Refers to the induced condensates agent

in – Entering the reactor

m.f. – Refers to minimum fluidization conditions

N_2 – Nitrogen

out – Exiting the reactor.

p – Refers to the polymer particle.

PE – Polyethylene.

pol – Refers to the polymer

polym – Polymerization

ref – Reference

s – Refers to the solids in the reactor

t – Refers to terminal conditions

v – Volumetric

0 – Initial condition

Superscripts

P – Refers to the polymer phase

* – Concerns the catalyst active sites

Glossary

CSTR – Continuous Stirred Tank Reactor

EOS – Equation of State

FBR – Fluidized Bed Reactor

HDPE – High Density Polyethylene

ICA – Inert/Induced Condensing Agent

LDPE – Low Density Polyethylene

LLDPE – Linear Low Density Polyethylene

MWD – Molecular Weight Distribution

MW – Molecular Weight

PC-SAFT – Perturbed Chain Statistical Association Fluid Theory

PSD – Particle Size Distribution

RTD – Residence Time Distribution

This page was intentionally left blank.

0. Thesis Outline

This thesis is divided into the following chapters: Introduction, Literature Review, Model Implementation, Results and Conclusions.

In the **Introduction**, general information about polyethylene and short overview of polyethylene integrated in the polyolefin industry will be presented. Afterwards the objective of the thesis will also be clarified.

The **Literature Review** will present the necessary information that allows the reader to understand the subjects regarding this work. It is divided into three main sections:

- The first will contain a common background, describing the general processes for the industrial production of polyethylene.
- The second focuses on describing a gas-phase fluidized bed reactor for the production of polyethylene. This includes the reactor behavior and the effects of the induced condensed agent. A quick overview of the previously developed models is also presented.
- The third part focus on the particle sizes distribution and how the polymer particles grow.

The chapter **Model Description** will be divided into two subchapters: Model equations and Model Implementation. The first subchapter will include the assumptions and equations used in the model. The subchapter Model Implementation will thoroughly explain how the model was implemented.

The **Results** chapter will be divided accordingly to the type of simulation: model validation, model simulations and sensitivity analysis.

The final chapter, **Conclusions** will include the main conclusions of this work and will finish with suggestion for further improvements.

1. Introduction

1.1. Properties of Polyethylene

Polyethylene (PE) is a polyolefin consisting, in its simplest form, of a long backbone chain with an even number of carbon atoms (covalently linked) and two hydrogen atoms attached to each carbon, ending in methyl groups [1].

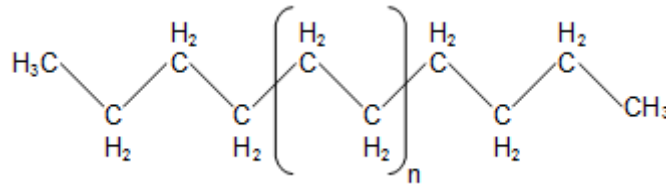


Figure 1.1. Polyethylene chemical structure. Adapted from [1].

A chemically pure polyethylene presents the chemical formula $C_{2n}H_{4n+2}$, where n is the degree of polymerization. This polymer consists of molecules of different sizes (and occasionally composition), wherein the degree of polymerization can vary and go as high as 250000. This means that its molecular weight varies from 1400 to 3500000 grams per mole or more, which leads to the resulting polymer presenting a molecular weight distribution (MWD). Some degree of branching and unsaturation can also be observed in the polymer molecules [1].

Polyethylene is often classified according to its melt flow index and density.

The melt flow index (MFI) is related to the molecular weight and processability of the product. A higher MFI polymer will typically have a lower molecular weight and processes easier than a polymer with lower MFI [2].

The density of the polymer reflects its crystallinity. If the main polyethylene chain presents many branches, it won't be neatly packed and the final product will present lower density and crystallinity. Polyethylene resins can be organized into three main categories: high density polyethylene (HDPE), low density polyethylene (LDPE) and linear low density polyethylene (LLDPE).

Polyethylene is considered **HDPE** if its density is between 0,945-0,970 g cm³. These resins present the highest density and crystallinity in the PE family. They present minimal branching and linear chains that may be obtained by slurry, solution or gas-phase processes. HDPE presents a different molecular weight distribution (MWD) according to the catalyst used. More HDPE properties are presented in Table 1.1. [2][3]

It is most commonly used in household containers and piping. The Figure 1.2 describes the different downstream processes/application of HDPE.

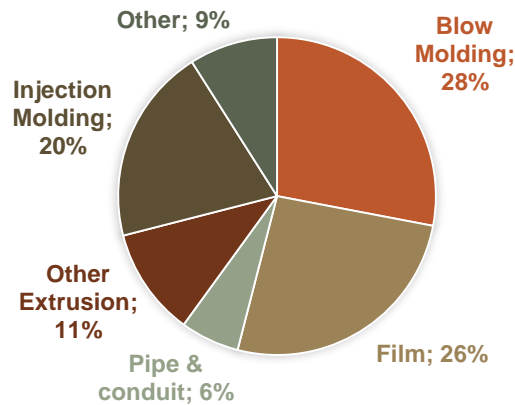


Figure 1.2. Main downstream processes/applications of HDPE in 2007. Adapted from [4].

HDPE films are very thin resins with applications in packaging (such as shopping bags) and product protection, such as powders, food or electronic parts [2][4].

Polyethylene is considered **LDPE** when its density is between 0,915-0,940 g cm³. These resins are non-linear chains with random short and long branching. They lack crystallinity which leads to end use applications to be flexible. They are produced under high pressures, so autoclave e tubular reactors are preferred. Figure 1.3 below illustrates the main applications of LDPE. More properties are presented in Table 1.1 [2][3][4].

Polyethylene is considered **LLDPE** when its density is below 0,930 g cm³. These resins are linear with short random branching. As HDPE, LLDPE can also be produced using solution, slurry or gas-phase reactors. Most commonly it is produced in gas-phase by copolymerization of ethylene with an α -olefin, under much lower pressure than LDPE. Even though LDPE and LLDPE present similar density ranges, their properties are very different. LLDPE presents a narrow MWD which leads to a product with better tear and impact film properties than LDPE. The main applications/downstream processes of LLDPE are displayed in Figure 1.3. More LDPE properties are presented in Table 1.1 [2][4].

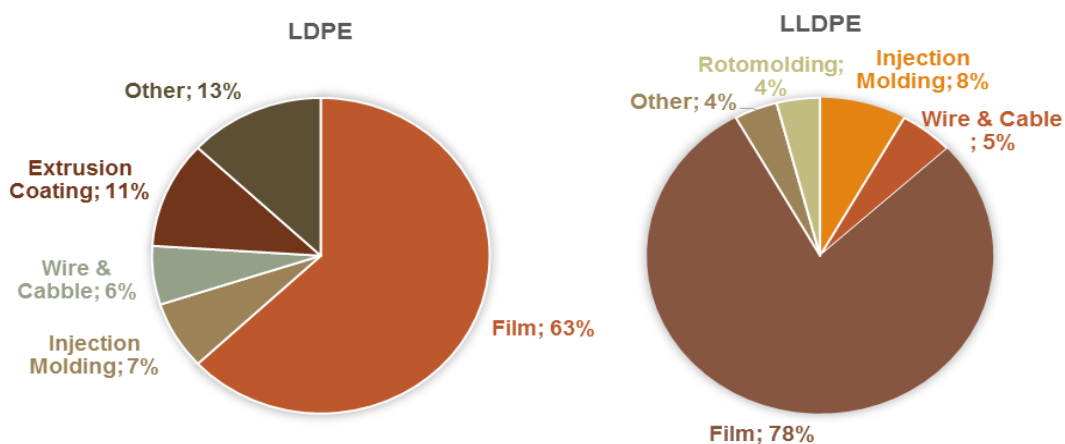
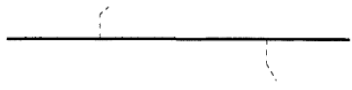
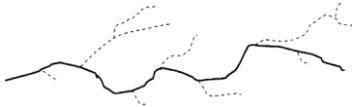
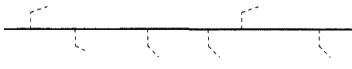


Figure 1.3. Main downstream processes/applications of LDPE (right) and LLDPE (left) in 2007. Adapted from [4].

The main application of LDPE and LLDPE is film.

Table 1.1 summarizes the main properties of polyethylene and contains a schematic representation of the different types of polyethylene.

Table 1.1. Summary of the properties of PE categorized by density. All figures adapted from [4].

Schematic Representation	Density (g.cm ⁻³)	Crystallinity degree (%)	Properties
<p style="text-align: center;">HDPE</p> 	0,945 to 0,970	60 to 65	<ul style="list-style-type: none"> • White opaque rigid solid; • Low level of long and short branching; • MWD depends on catalyst
<p style="text-align: center;">LDPE</p> 	0,915 to 0,940	45 to 55	<ul style="list-style-type: none"> • Translucent flexible solid; • Random long branching; • Broad MWD.
<p style="text-align: center;">LLDPE</p> 	< 0,930	30 to 45	<ul style="list-style-type: none"> • Translucent flexible solid; • Branching with uniform length randomly distributed across the linear chain; • Narrow MWD.

1.2. Polyethylene Worldwide

Polyethylene is the most widely produced thermoplastic in the world, representing 37% of the entire polymer demand in 2012 (Figure 1.4). In 2008, 44% of polyethylene consumed was high density polyethylene (HDPE). In the same year, 29% of the consumed polyethylene was linear low density polyethylene (LLDPE) and the remaining 27% were low density polyethylene (LDPE).

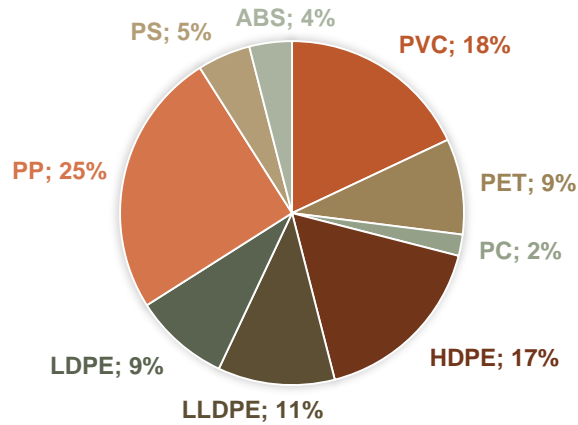


Figure 1.4 – Demand for total polymer in 2012. Adapted from [5].

Polyethylene's market has been growing since it first started to be commercialized and is still growing at a rate of 5% annually [4]. Figure 1 shows the market growth for all polyethylene products since 2004, including a future prospect until 2017.

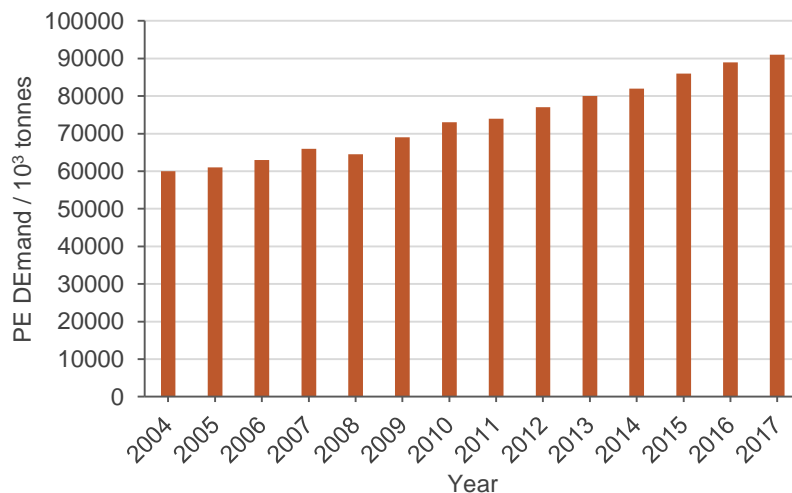


Figure 1.5 – Growth of Polyethylene's demand and future prospects. Adapted from [5].

1.3. Polyethylene Production

Polyethylene is produced using ethylene as a monomer. Ethylene is generally obtained from steam cracking of crude oil derivatives, so it is very common to find a petrochemical complex with a refinery, a cracker and a polymer plant all in one site. This represents a high capital investment to produce polyethylene. Since the final product is often very low cost, increasing production and lessening material cost have become a priority [6].

The reactors for the production of polyolefins, such as PE, can be divided into three main types, broadly speaking: **solution** (homogenous catalyst), **slurry** and **gas-phase** (both heterogeneous catalyst). In the slurry approach the gaseous/liquid feed monomers are paired with a diluent (carbohydrates C4-C6) in which the catalyst particles are suspended. Slurry

processes like this require the use of autoclave or loop reactors. The gas-phase process uses fluidized bed reactors (FBR). The gaseous stream of monomers and inerts (nitrogen) fluidizes the bed of polymers particles in a FBR and creates good heat transfer conditions. This works focuses only in the production of PE in gas-phase, without to any further mention of the production of polyolefins with solution and slurry processes.

The biggest concerns when designing a polymerization reactor is the need to remove the heat of reaction in an efficient manner so that the reaction is fully controlled. Polymerization reactions are highly exothermic. This leads to a temperature increase inside the reactor and consequently to production rate problems. In the production of LLDPE only a gas-phase can be considered, given that the amorphous phase of this polymer is dissolves in the diluents used in slurry processes. For both of these reasons, only gas-phase reactors are considered when producing PE. Since the heat released in this particular polymerization reaction is very high, FBRs are usually preferred [2].

1.4. Motivation

The subjects discussed in the last section highlight the importance of polyethylene worldwide. Since PE is a part of the petrochemical industry and the available predictions point to an undisputed growth of the demand for this product, further development is of the utmost interest.

2. Literature Review

2.1. General information on the Polyethylene Industrial Process

To better understand the polyolefin industry it is necessary to discuss the different processes available. Since there are so many different polymer grades with distinctive molecular weight distributions, compositions and branching, it is obvious that a wide range of processes and operating conditions are available.

The output of polymerization processes has drastically increased over the years. In the 1960s the yearly capacity was about 80 ktonnes and increased to an impressive 750 ktonnes in modern facilities. This radical change is mostly due to increased operation efficiency [2].

A general description of an industrial polymerization unit is shown in Figure 2.1.

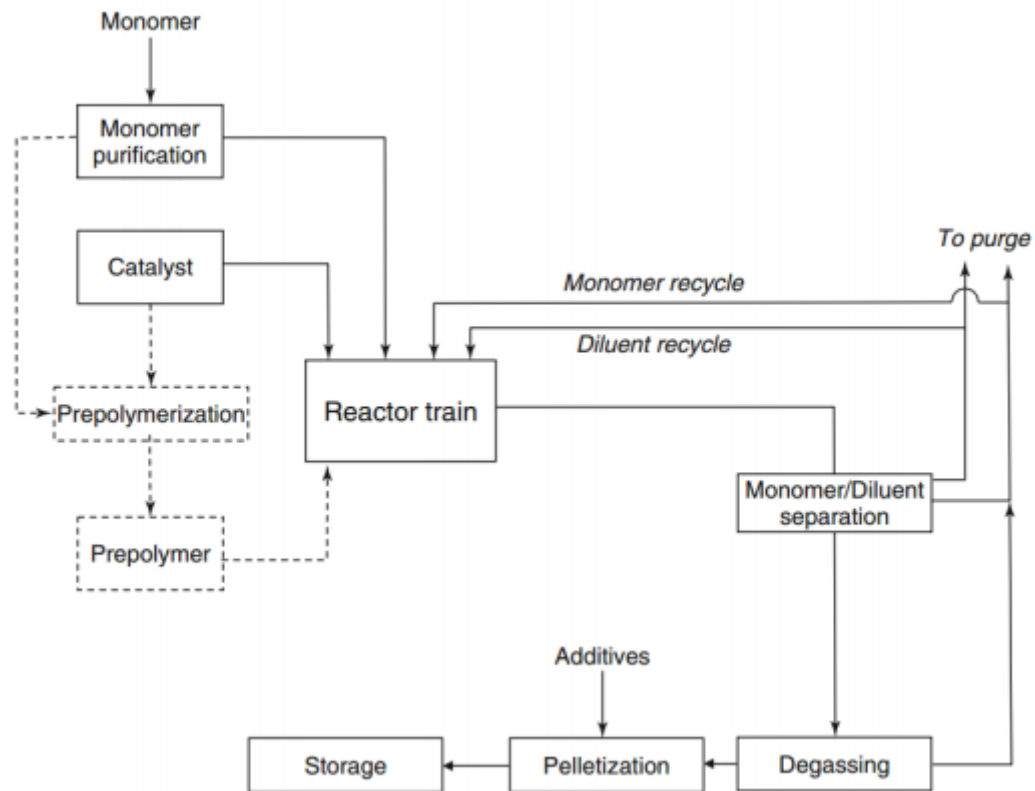


Figure 2.1. Schematic representation of the a polyolefin production unit (adapted from [2]).

The monomer, catalyst and other process fluids are fed to the reactor train. In some processes, there is the need to prepolymerise the catalyst for better particle morphology before entering the reactor. Exiting the reactor train, the polyolefin and process fluids are separated. The recovered diluent (if used) and monomer are recycled to the reactor train, after being purged. The recovered polymer then undergoes several operations, such as degassing and palletization, before being stored.

It is important to mention that this general process prevails in the production of all kinds of polyolefins, diverging mainly in the reactor type and the medium in which the particles are suspended.

2.2. Gas-phase Reactors

Gas-phase reactors are often used for the production of HDPE and account for over 20 % of the world polyethylene capacity [3]. They are very economical, since the separation of unreacted monomers from the polymer is relatively easy. The major disadvantage with these reactors is the difficulty associated with the heat removal. Since it is gas-phase, the overall heat transfer properties are very poor, therefore space-time yields are lower than in slurry processes. Extra steps must be taken in order to keep these reactors economically feasible. Addition of small amounts of liquid components below their dew point or of inert gases with elevated heat capacities are the most common solutions for this problem. Due to the heat removal difficulties, the **fluidized bed reactors** are preferred for the production of polyethylene in gas-phase processes [4][7].

The first implementation of FBR technology was by Union Carbide. The main advantage of this process, other than the easy separation of the polymer/gaseous stream, is that this is a true swing process. This means that the same process can be used to produce resins with an array of grades, from LLDPE to HDPE. The following Figure 2.2 illustrates the process.

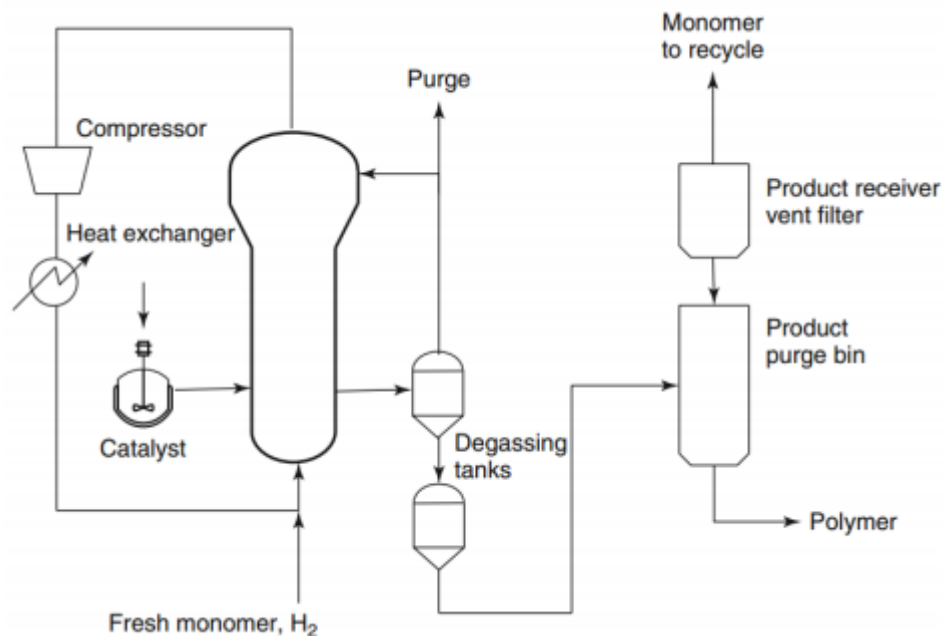


Figure 2.2. Unipol Process for PE production (adapted from [2])

This configuration is similar to the one seen in Figure 2.1, in the sense that fresh monomer and catalyst are added to the reactor. In the reactor outlet a stream of polymer and gas is recovered, being degasified afterwards. The polymer can then undergo additional operations and treatments while the gas phase is purged and recycled.

The following Table 2.1 gives an overview of some existing gas-phase processes. Most consist of 1 or 2 FBR with similar ranges of pressure and temperature.

Table 2.1. Typical reactor conditions for gas-phase HDPE processes (adapted from [2][8][9]).

Process	Reactor Type	Mode of operation	Reactor Temperature (°C)	Reactor Pressure (bar)	Residence time (hours)
Unipol	1 or 2 FBR	Condensed	90-110	20-25	2
Spherilene	1 FBR	Condensed	90-110	20-25	2
Spherilene	1 or 2 FBR	Dry	70-90	20-25	1.5
Innovene G	1 FBR	Condensed	90-110	20-25	2

A typical FBR looks like the one shown in Figure 2.3. The polymer particles grow by polymerization at low temperatures (70-90°C) and pressures (20-30 bar). The reaction occurs in a fluidized bed, sustained by the upward flow of gaseous monomer and co-monomer. The process allows C₈, C₆ and C₄ co-monomer flexibility. In addition, it may include a cyclone that removes the need for regular loop cleaning and reduces grade transition time. These processes rely on the use of Ziegler-Natta and metallocene catalysts [2][8].

The biggest difference between the processes shown in Table 2.1. is the reactor operation mode. The operation can be carried out in dry or condensed mode. The FBR shown in Figure 2.3. operates in condensed mode, in which the reactor feed is made of a liquid (Induced Condensed Agent - ICA) in equilibrium with the gas-phase. This allows to further enhance heat removal, by increasing the gas heat capacity with a heavy inert alkane and to remove sensible heat with the evaporation of the liquid. In dry mode the heat removal problem is solved by increasing the gas heat capacity with the introduction of a heavy inert alkane or with a co-monomer.

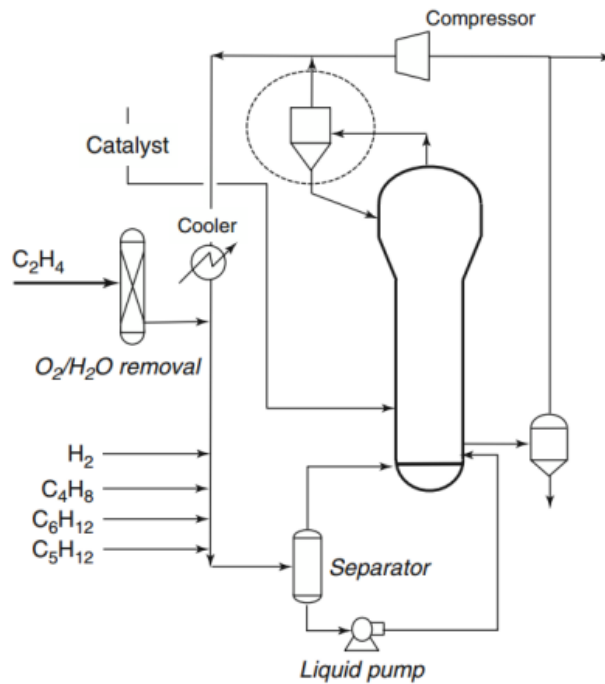


Figure 2.3. Innovene G process from INEOS (adapted from [2]).

2.2.1. Fluidized Bed Reactors for Polyethylene Production

The FBR is simply a vessel with a distributor plate at the bottom and a separation area at the top. Even though cooling of the walls occurs, only a small amount of heat is removed through them. For this reason, these reactors are often considered adiabatic. The polymerization reaction takes place between these two areas. The feed, composed of ethylene, hydrogen, nitrogen, possibly a co-monomer and/or more alkanes are injected below the distribution plate which orients the gases in a manner to promote bed fluidization. The reaction zone begins after the distribution plate, near the same height as the polymer particles are withdrawn (see Figure 2.4, below). Just above the distribution plate and below the polymer recovery, the fresh catalyst is injected.

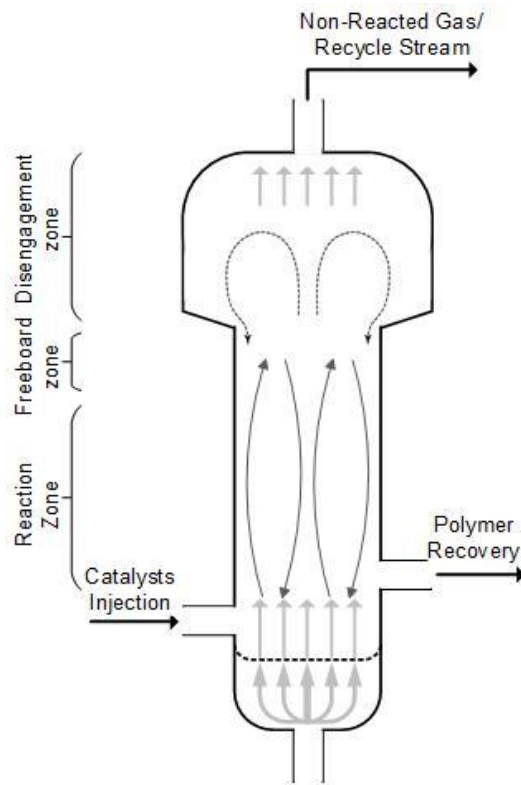


Figure 2.4 - Diagram of a fluidized bed reactor for PE production. Adapted from [2].

The gas flow rate in this reactor must be sufficient to ensure bed fluidization as the polymer grows around the catalyst, so superficial rates between $0.5-1 \text{ m.s}^{-1}$ are observed. The relative gas-particle rate is 2-8 times bigger than the minimum fluidization rate. This implies large flow rates; which are achieved by using recycling ratios up to 50, with lower per pass conversion 5-30%. The recycled gas is first recovered at the top of the bed then compressed and cooled, before being fed back to the reactor. With this relative gas-particle velocity, the heat removal is much easier in fluidized bed reactors than in stirred bed. This explains the preferred option for polyethylene production in gas-phase.

The reaction zone is separated from the disengagement zone by the freeboard zone. Here the void fraction is approximately one, while the velocity of most particles will go down to the minimum of fluidization and fall back into to the bed. However, there are particles that are too small and get dragged out of the freeboard zone into the disengagement zone.

The top of the reactor, known as the disengagement zone, has at least twice the diameter of the rest of the reactor. By enlarging the diameter, the superficial rate drops drastically retaining most of the dragged out particles. However, there is still a fraction of lost particles.

In the regular smooth FBR's the gas flow can be compared to a plug-flow. The powder is pushed into the center of the reactive bed and falls down along the outside walls, forming a recirculation zone. A full cycle takes between 30-60 s to be completed, which gives RTD's of 30-180 min when it is likened to an CSTR [2].

Reactor pressure and temperature are chosen as a trade-off between operability and desired polymer properties and production rates. In the case of polyethylene, the softening temperatures are close to 90° C for LLDPE and 110° C for HDPE. The thermal sensitivity of the catalyst will also play a role in choosing the adequate reactor temperature. A stable temperature is of the utmost importance in this process. The presence of hot spots and fine particles (diameter below 100 µm) are major issues. Fine particles have higher heat removal problems and hot spots lead to the particles melting and sticking together, both forming minor lumps and chunks, which may lead to problems in downstream processes or clog the reactor outlet.

As mentioned above, heat removal is one of the keys elements in PE production. With a heat of reaction in the order of 100 kJ/mole PE, a commercial unit generates tons of megawatts of energy during the polymerization process [2]. Predominately, most of the heat is removed via the gas phase. Increasing the gas flow rate improves the relative gas-particle velocity, which leads to a higher heat transfer coefficient. This step is much easier in a FBR than in any other gas-phase reactor. However, there are some limitations on the increase of the gas flow rate, since the bigger the rate, the smaller the conversion for each pass and bigger the recycle ratios. Increasing/decreasing the superficial velocity can be complex. The minimum fluidization velocity must be guaranteed so there is no collapse of the fluidized bed, but at the same time a high superficial velocity can pneumatically transport the particles. Another mean of increasing the gas ability to remove heat is by changing the gas thermal properties. This happens, in the case of the ethylene polymerization, by adding an alkane, such as propane, butane or hexane. The added alkane is referred to as an Induced Condensing Agent (ICA) when the reactor works in condensed mode. This term will be used for both condensed and uncondensed alkanes to simplify notation.

Table 2.2 shows the ranges of operating conditions usually applied in this process.

Table 2.2. FBR operating conditions for HDPE production [2][3][10].

Pressure (bar)	20-30	Polymer density (g.cm ⁻³)	0.91-0.97
Temperature (°C)	70-110	MW control agent	H ₂
Catalyst size (µm)	30-130	Residence time (h)	1-4
Polymer Particle size (µm)	300-1300	Superficial Velocity (m/s)	0.5-1
Per pass conversion (%)	3-30	Reaction bed height (m)	10-15
Overall conversion (%)	>95	Bed height/diameter ration	2.5-5

2.2.1.1. *Dry Mode Operation*

When only gas is present in the inlet stream, sensible heat removal is only possible by transferring heat into the gas phase and the reactor operates in dry mode. In addition to increasing the gas flow rate, chilled feeds are also another way to empower heat removal. In this case, there is the need for an external heat exchanger. The presence of an ICA can extend the gas-phase

heat capacity, increasing the gas ability to remove heat. Figure 2.5 shows a diagram for the dry-mode process [2][7].

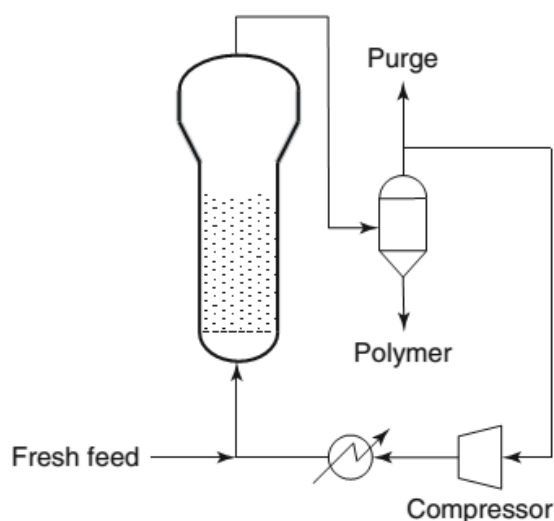


Figure 2.5 - Diagram of feed, recycle and cooling of the gas in an FBR (adapted from [2]).

In the case of using a chilled feed, the gaseous stream is cooled down after compression and mixed in with the fresh feed stream.

2.2.1.2. **Condensed Mode Operation**

If a condensed material is included in the recycle stream, then the reactor is working in condensed mode. The recycle stream can be cooled down below dew point, providing the reactor feed with a gas in equilibrium with a liquid. The liquid ICA vaporizes inside the reactor to further remove heat. This way, the condensable material not only removes sensible heat, but also latent heat during the vaporization process. The process of heat removal with the latent heat of vaporization is extremely efficient and can greatly increase the reactor throughput (more than twice the throughput of the dry mode). Changing the composition of the condensable phase allows to custom tailor the dew point to each reactor and operating conditions. Although this process is economically feasible, adding an inert alkane will increase the downstream separation and purification costs. One must also be careful when operating in this mode, to not disturb the FBR behavior and ensure that there are no large droplets in the bed. In most cases, the liquid is sprayed by the distribution plate and is all vaporized within the first 1-2 m [2][7].

2.2.2. **Overview of the Induced Condensed Agents**

An Induced Condensed Agent (ICA) is a C_3 - C_8 hydrocarbon, introduced in the reactor feed to aid heat removal [11]. The ICA can be introduced as a gas or in a gas/liquid equilibrium. The initial purpose of adding ICA to the reactor is to regulate the liquid stream dew point and/or increase vapor stream heat capacity. However, there is another noticeable consequence of great interest as well: the ICA is considerably absorbed by the polymer phase. This absorption is observed to be primarily a function of the fraction of ICA in the gas phase, but also a function of

the amorphous phase polymer density. This phenomena has two main consequences: it alters the polymer physically and it changes the ethylene/polymer equilibrium [11][12].

The adsorption of ICA into the polyethylene is observed to modify the polymer physically, by swelling and plasticizing it, as well as increasing its density. Furthermore, the ICA influences the characteristics of the polymer crystalline phase, such as crystallinity and lamellar thickness [13]. Additionally, the ICA functions as a delaying agent for the crystallization kinetics during polymer growth. Even though no information in the open literature is available, it is expected that the plasticization of the polymer and the increase in the polymer density, may make the polymer more resistant to breakage. It may also allow some particles to re-agglomerate [11][13].

The adsorption of ICA may also buffer temperature swings in growing particles [11]. Although fluidized bed processes have a good uniformity of temperatures, there are still regions of uneven temperature, specifically: near the feed inlet, along the vessel walls and in the disengaging zone. Additionally, there are temperature gradients within the individual particles when they are actively producing polymer. The equilibrium absorption of the ICA into the polymer decreases with the increase of temperature. The desorption involves a latent heat similar to evaporation. Thus, when particles reach a hot region and begin to overheat, some ICA will desorb from the polymer, causing a cooling effect. Conversely, when the particles are found in the cool zones, there will be a rise in ICA absorption, causing a latent heat of absorption that will, in some measure, counteract the cooling effect [11]. Again, without any confirmation in the open literature, it is possible that this behavior dampens the thermally induced activity swings and stress in the particles, reducing their tendency to breakage [11].

The adsorption of ICA in the amorphous polymer phase can also effect the mass diffusion in the polymer. The ICA presence widens the polymer particles, aiding the transport of components in and out of the particles. This is of the utmost importance, since the vast majority of the active sites are not in the outer surface of the catalyst/polymer particle. Thus, polymer micro-particle clusters may grow within the particle, with polymer macro-particles surrounding and enveloping the catalyst particles. Therefore, the delivery and withdrawal of species having a relatively high thermal conductivity may become a mechanism of cooling the micro-particle clusters [12].

The polymer/ICA/ethylene system has an interesting interaction between the different components, especially when analyzing the effect that the ICA has on the ethylene solubility in the polymer. To study this system interactions, a thermodynamic model is required to properly describe them. Due to the non-ideality of the polymer-penetrant thermodynamics, it is necessary to employ a model that is able to give an accurate prediction of the monomer and the ICA concentration in polymer phase. However, these types of model are difficult to obtain, since they are semi-empirical. Therefore, they require experimental data, which is both difficult and expensive to acquire. Linear models, such as Henry's Law are not enough to even approximately

describe the complex phenomena taking place due to the intricate interactions between penetrants [2][10].

In the open literature, it was found that two main models are applied in the polymer industry: Perturbation theory models, such as the **Perturbed Chain Statistical Association Fluid Theory** (PC-SAFT) and lattice models such as the **Sanchez-Lacombe Equation of State** (SL-EoS) [10]. The latter model was used in the present work and is described in more detail in Appendix A.

The presence of ICA leads to the increase of ethylene concentration in the polymer phase. In addition, the higher the carbon number of the ICA the higher the ethylene concentration in the polymer phase at the same conditions. This observation can be attributed to the co-solvent effect of alkanes on the solubility of ethylene which manifest itself in multicomponent gases/polymer systems and is well known in the open literature [14][15][16][17]. It is important to mention that no specific reason has been provided in the open literature for the occurrence of the co-solubility effect.

2.2.3. Previous Models

Since FBR's are widely used in many forms, one can find many models for predicting their behavior in the open literature [18],[19],[20]. Such studies describe fluidized beds in great detail and are provide an extensive list of empirical correlations which may be used to estimate properties of importance when designing fluidized bed reactors.

Studies on the modelling of FBRs in the specific case of PE production are extremely numerous as well, and exhibit many levels of complexity. For example, Choi and Ray [21], and Grosso and Chiovetta [22] proposed a two-phase model of a bubbling FBR that is able to track temperature and concentration gradients in the reactor assuming a constant bubble size. Other groups extended this analysis to include variable bubble sizes with a uniform emulsion phase [23] with regard to the temperature and concentration gradients in the gas phase. Even more complex models have been developed that divide the different phases into separate zones in order to obtain a more accurate picture of the gradients as well as of the particle size distribution in the reactor [2]. However, very few studies in the open literature have taken the impact of adding ICA into account. As such, there is a big uncertainty associated with this mode of operation. The McAuley's simplified approach to treat the powder phase of an FBR as a continuous stirred tank reactor in terms of the residence time distribution, and ignoring temperature gradients in the gas phase will be considered valid [24].

The present work is based on two existing models developed by Cecílio [25]. The author proposes a simple model for the reactor, built on simplified mass and heat balances and on a replica of a PSD model previously developed by Soares *et al.* [26].

2.3. Particle Size Distribution

The particle size distribution (PSD) refers to the categorization of the number of particles that exhibit the same size. The knowledge of the polymer PSD allows to better design and operate polymer recovery, treatment and processing units [22][26].

2.3.1. Particle Fragmentation and Growth

The supported catalysts used in the polyolefin industry are highly porous particles with typical diameters in the order of 10–100 μm [2]. The supported catalyst particle (macrograin or macroparticle) is composed of an assembly of smaller structures, often referred to as micrograins (also called microparticles) [2][27][28]. While interest in other support types is growing, MgCl_2 and SiO_2 are essentially the only commercially used supports at present.

The particle growth begins with a process referred to as **particle fragmentation**. As shown in Figure 2.6., when the particles are fed into the reactor, monomer, hydrogen, and any other species present in the continuous phase of the reactor begin to diffuse into the particle pores. As soon as the reactive species reach the active sites, they start to react, forming polymer layers inside the pores of the catalyst particle, and the structure, or morphology, of the particle begins to evolve. As polymer accumulates at the active sites, the inorganic phase suffers a local buildup of stress at different points, and very quickly fragments into a series of unconnected mineral substructures held together by a polymer phase. This process continues throughout the entire support as monomer keeps reaching the active sites and polymer builds up. This kind of fractioning is well known and described in several references [28][29][30][31].

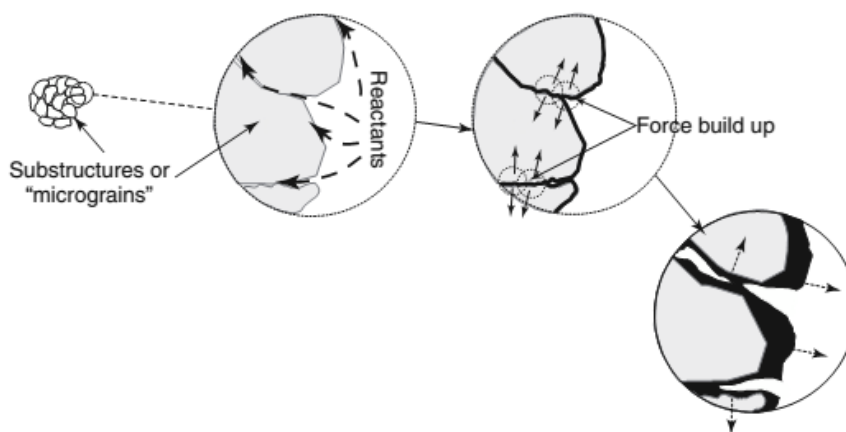


Figure 2.6. Particle growth evolution. Adapted from [2].

One consequence of this catalyst fragmentation mechanism is the replication phenomenon, where the PSD shape of the polymer particles is duplicated by the polymer PSD. This is a very important phenomenon, since it allows to easily predict the polymer PSD. Good replication requires a balance between the mechanical strength of the particle and catalyst

activity: If the particle is too weak, it will break as the polymer starts to branch and form undesirable fine particles; if the particle is too resistant there will be little or no fragmentation and the polymer chains will block the catalyst pores, making the internal active sites inaccessible to monomers [2][26][32].

Once fragmentation occurs, the **particle growth** step begins. The polymer particle grows by expansion: the newly formed polymer at the active sites displaces the previously formed polymer [2].

2.3.2. Previous Models

There are several models in the open literature that describe the particle growth and final size distribution. The work developed by McAuley *et al.* [33] and Talbot [34] consider that the distribution inside the reactor is equal to the exiting stream. This is a contrast with the work developed by Grosso and Chiovetta [22]. These authors introduce the restriction posed on the overall polymerization process by the particle system separation in the discharge chamber. The model recognizes the fact that the chamber was added to ensure that only the larger particles exit the reactor. This enforces a polymer PSD at the exit point [22].

3. Model Description

In this chapter the model assumptions, equations and implementation are presented.

The present model consists of the merging and upgrading of two existing models developed by Cecilio [25]. The base models consist of a Particle Size Distribution (PSD) model and a gas-phase polyethylene FBR model. The PSD model calculates the PSD of the polymer particles produced with heterogeneous Ziegler-Natta catalysts. The model developed by Cecilio [25] is adapted for a slurry phase reactor. However, a simple adaptation can be made to apply the same model in FBR's. The reactor model emulates the behavior of a FBR reactor for the production of polyethylene.

The model presented in the following section describes the operation of a gas-phase HDPE production reactor in dry mode through a series of mass and heat balances. The description will be divided into different sections that are based on the main categories of equations present in the model: **mass and heat balances**, **PSD and mean particle size calculation** and **bed porosity and pressure drop**. Other calculations in this work include gas-phase properties and are presented in Appendix B.

The mass and heat balances in the present model are based on a set of problem definitions and assumptions, described below.

Problem Definition:

- 1 gaseous inlet consisting of ethylene, an inert heavy alkane and nitrogen;
- 1 solid inlet stream consisting of catalyst particles;
- 1 gaseous outlet containing non-reacted ethylene, inert heavy alkane and nitrogen;
- 1 solid outlet containing the polymer phase, consisting of the polymer and catalyst particles with dissolved ethylene and alkane;
- Due to the heat transfer, 2 different outlet temperatures are considered, one for the gaseous outlet and another for the polymer phase outlet;

Assumptions:

- The residence time distribution of the particles is assumed to be that of an CSTR operating in steady-state;
- The catalyst particles are considered spherical;
- Catalyst activation is considered to be instantaneous;
- Elutriation of solids is neglected;
- The thermodynamic equilibrium is achieved instantaneously and the polymer particles are considered fully mature;
- The gas-phase keeps a constant concentration of ethylene, ICA and N₂;

- Ethylene and ICA solubility dependence on temperature is neglected within each range of temperature;
- Nitrogen solubility in the polymer phase and impact on ethylene solubility are neglected;
- Convective heat transfer is considered between the catalyst/polymer particles and the bulk gaseous phase, which results in the existence of two different temperatures (bulk and solids)

As discussed in chapter 2, approximating an FBR by a CSTR RTD is a reasonable first approximation. The RTD of the powder phase in an FBR is similar to that of a CSTR. This implies a great number of assumptions associated with CSTR reactors. The restraining of the components present in the inlet and outlet flows is due to the constraints of the Sanchez-Lacombe thermodynamic model, since it can only give reasonable predictions for a ternary system, including the polymer. Also related to Sanchez-Lacombe thermodynamic model restrains, the impact of different degrees of crystallinity on ICA solubility will be ignored. While this is not desirable, the monomer and alkane can only diffuse in the amorphous part of a polymer and it appears that the impact of polymer crystallinity is a second order effect. Considering that the equilibrium is established instantaneously translates into neglecting mass diffusion resistances.

3.1. Model Equations

3.1.1. Mass Balances

3.1.1.1. Ethylene Mass Balance

The general form of the ethylene mass balance is written as follows:

$$Q_{Et,in} - Q_{Et,out} - R_p(T, P) \cdot V_c \cdot MW_{Et} - Q_{Et,d} = 0 \quad (3.1)$$

Where $Q_{Et,in}$ is the ethylene mass flow rate entering the reactor ($\text{kg}\cdot\text{s}^{-1}$), $Q_{Et,out}$ is the ethylene mass flow rate exiting the reactor (kg/s), R_p is the reaction rate at a given temperature and pressure ($\text{mol}\cdot\text{m}^{-3}\cdot\text{s}^{-1}$), V_c is the catalyst volume (m^3) and $Q_{Et,d}$ is the flow rate of ethylene dissolved in the polymer phase ($\text{kg}\cdot\text{s}^{-1}$). This last variable can be defined as:

$$Q_{Et,d} = \frac{C_{et}^p \cdot MW_{Et}}{\rho_{pol}} \cdot Q_{PE} \quad (3.2)$$

Where C_{et}^p is the concentration of ethylene in the polymer phase ($\text{mol}\cdot\text{m}^{-3}$) and Q_{PE} is the PE production rate ($\text{kg}\cdot\text{s}^{-1}$).

The ethylene per pass conversion is given by equation (3.3) and describes the fraction of monomer that reacts per cycle of gas stream. The dissolved ethylene is taken into account in equation (3.3) since only a very small amount of ethylene is dissolved in the polymer phase.

$$\text{Conversion (\%)} = \frac{(Q_{Et,in} - Q_{Et,out})}{Q_{Et,in}} \cdot 100 \quad (3.3)$$

3.1.1.2. ICA Mass Balance

The general form of the alkane heat balance is given as:

$$Q_{ICA,in} - Q_{ICA,out} - Q_{ICA,d} = 0 \quad (3.4)$$

Where $Q_{ICA,in}$ is the ICA mass flow rate entering the reactor ($\text{kg}\cdot\text{s}^{-1}$), $Q_{ICA,out}$ is the ICA mass flow rate exiting the reactor ($\text{kg}\cdot\text{s}^{-1}$) and $Q_{ICA,d}$ is the flow rate of ICA dissolved in the polymer phase ($\text{kg}\cdot\text{s}^{-1}$). The $Q_{ICA,d}$ equation is similar to the ethylene:

$$Q_{ICA,d} = \frac{C_{ICA}^P \cdot MW_{ICA}}{\rho_{pol}} \cdot Q_{PE} \quad (3.5)$$

Where C_{ICA}^P represents the concentration of ICA in the polymer phase ($\text{mol}\cdot\text{m}^{-3}$).

3.1.1.3. Nitrogen Mass Balance

The nitrogen is a chemically inert gas, and its solubility in the polymer is neglected, reducing the mass balance to equation (3.6).

$$Q_{N_2,in} = Q_{N_2,out} \quad (3.6)$$

Where $Q_{N_2,in}$ and $Q_{N_2,out}$ represents the inlet and outlet flowrate of nitrogen ($\text{kg}\cdot\text{s}^{-1}$), respectively.

3.1.1.4. Reaction Rate and PE Production Rate

The reaction rate assumed for the polymerization was proposed by Floyd [35] and is written as follows:

$$R_p = k_p \cdot C^* \cdot C_{Et}^P \quad (3.7)$$

Where k_p represents the kinetic rate constant ($\text{m}^3\cdot\text{mol}^{-1}\cdot\text{s}^{-1}$), given by equation (3.10) and C^* is the active sites concentration on the catalyst ($\text{mol}\cdot\text{m}^{-3}$). This is given by equation (3.8), presented below.

$$C^* = \frac{C_0^*}{1 + k_d \cdot \frac{V_c}{Q_c}} \quad (3.8)$$

Where C_0^* is the initial active sites concentration ($\text{mol}\cdot\text{m}^{-3}$) and $\frac{V_c}{Q_c}$ can be interpreted as the catalysts residence time.

In equation (3.7) C_{Et}^P represents the ethylene concentration inside the amorphous polymer phase ($\text{mol}\cdot\text{m}^{-3}$). This parameter is of the utmost importance and an estimation is needed in order to predict the polymer production.

A thermodynamic model was implemented in order to estimate the polymer density and ethylene and ICA concentration in the polymer phase. As mention in Chapter 2, the chosen model was the Sanchez-Lacombe Equation of State (SL-EOS) (see appendix [A]), a widely applied model in the polymer industry.

It is important to mention the use of Arrhenius Law to predict catalyst deactivation (k_d) (s^{-1}) and the kinetic rate (k_p) ($\text{m}^3\cdot\text{mol}^{-1}\cdot\text{s}^{-1}$) constants at the reaction temperature:

$$k_d^{T_s} = k_d^{T_{ref}} \cdot \exp\left[\frac{E_a}{R} \cdot \left(\frac{1}{T_{ref}} - \frac{1}{T_s}\right)\right] \quad (3.9)$$

$$k_p^{T_s} = k_p^{T_{ref}} \cdot \exp\left[\frac{E_a}{R} \cdot \left(\frac{1}{T_{ref}} - \frac{1}{T_s}\right)\right] \quad (3.10)$$

The production of PE ($\text{kg}\cdot\text{s}^{-1}$) is estimated according to the following expression:

$$Q_{PE} = R_p \cdot V_c \cdot MW_{et} \quad (3.11)$$

The catalyst productivity ($\text{g}_{\text{polymer}}\cdot\text{g}^{-1}_{\text{catalyst}}$) is defined by equation (3.12):

$$Productivity = \frac{Q_{PE}}{Q_c} \quad (3.12)$$

3.1.2. Heat Balances

Inside the reactor two temperatures can be observed: The bulk temperature (T_b) and the solid particles temperature (T_s). Therefore, two heat balances are required, one to the solid particles and one to the reactor global heat.

3.1.2.1. Particles Heat balance

The heat balance to the solid particles can be written as follows:

$$\Delta H_{polym} = h \cdot A_p \cdot (T_s - T_b) \quad (3.13)$$

Where ΔH_{polym} is the heat of reaction ($\text{J}\cdot\text{mol}^{-1}$), h represents the convective heat transfer coefficient ($\text{W}\cdot\text{m}^2\cdot\text{K}^{-1}$) (see Appendix B) and A_p the heat transfer area (m^2), given by equation (3.14):

$$A_p = n_p \cdot \pi \cdot D_p^2 \quad (3.14)$$

Where n_p represents the number of particles and D_p the mean particle size diameter inside the reactor (m), obtained from the particle size distribution. The number of particles is obtained using the following expression:

$$n_p = \frac{6 \cdot V_{bed} \cdot (1 - \varepsilon_{bed})}{\pi \cdot D_p^3} \quad (3.15)$$

Where V_{bed} and ε_{bed} are, respectively, the fluidized bed volume (m³) and porosity.

3.1.2.2. Reactor Heat Balance

The reactor heat balance is written as follows:

$$\Delta H_{in} - \Delta H_{out} + \Delta H_{generated} = \Delta H_{accumulation} \quad (3.16)$$

Reference State:

- Reference Temperature – Inlet Temperature (T_{in});
- Reference Pressure – Reactor working pressure;
- Gaseous ethylene, nitrogen and alkane;
- Solid catalyst;
- Amorphous polyethylene.

Assuming this reference state and that the operation is occurs in steady state, the heat balance in equation (3.16) is reduced to:

$$-\Delta H_{out} + \Delta H_{generated} = 0 \quad (3.17)$$

Replacing the parameters, the equation (3.17) takes the following form:

$$\begin{aligned} Q_{Et,out} \cdot \overline{C_{p,Et}} \cdot (T_b - T_{in}) + Q_{ICA,out} \cdot \overline{C_{p,ICA}} \cdot (T_b - T_{in}) + Q_{N_2,out} \cdot \overline{C_{p,N_2}} \\ \cdot (T_b - T_{in}) + Q_{PE} \cdot \overline{C_{p,PE}} \cdot (T_S - T_{in}) + Q_C \cdot \overline{C_{p,C}} \cdot (T_S - T_{in}) \\ + Q_{Et,reacts} \cdot \Delta H_{polym} = 0 \end{aligned} \quad (3.18)$$

Where $Q_{Et,reacts}$ represents the ethylene flowrate that is consumed as a reactant (mol.s⁻¹):

$$Q_{Et,reacts} = \frac{Q_{PE}}{MW_{et}} \quad (3.19)$$

ΔH_{polym} is the polymerization reaction heat (J.mol⁻¹).

3.1.3. Bed Porosity and Pressure Drop

The pressure drop was calculated using Ergun's equation [36].

$$\frac{\Delta P}{L} = 150 \cdot \frac{(1 - \varepsilon_{mf})^2}{\varepsilon_{mf}^3} \cdot \frac{\mu \cdot u_{mf}}{d_p^2} + 1.75 \cdot \frac{(1 - \varepsilon_{mf})}{\varepsilon_{mf}^3} \cdot \frac{\rho_{gas} \cdot u_{mf}^2}{d_p} \quad (3.20)$$

Where ΔP is the pressure drop (Pa), L is the bed height (m), ε_{mf} is the porosity of the bed at minimum fluidizing conditions, μ is the gas viscosity (Pa.s), ρ_{gas} is the gas density (kg.m⁻³) and d_p is the particle diameter (m).

The superficial velocity, u_{mf} , is the minimum superficial gas velocity at which fluidization occurs. According to [20], the u_{mf} (m.s⁻¹) is given by equation (3.21).

$$u_{mf} = 0.00144 \cdot \frac{g \cdot d_p^2 \cdot (\rho_p - \rho_g)}{\mu} \quad (3.21)$$

In which ρ_p is the particle density (kg.m⁻³) and g is the gravitational acceleration constant (m.s⁻²).

The terminal velocity of the particles (u_t) (m.s⁻¹), which is the velocity at which transport occurs can be obtained from the following ratio [20]:

$$R = \frac{u_t}{u_{mf}} = 26.6 - 2.3 \cdot \log(Ar) \quad (3.22)$$

For Archimedes number between $4 \times 10^4 < Ar < 8 \times 10^6$.

The porosity of the bed was predicted in a simplistic fashion by taking advantage of the linear relationship between the superficial velocity and the bed porosity.

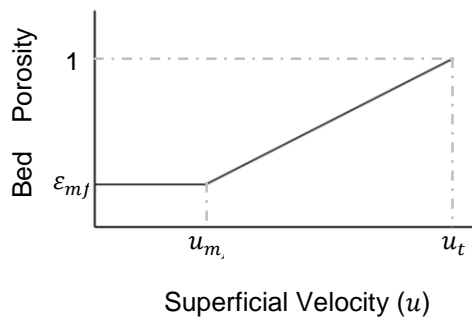


Figure 3.1 Bed porosity vs Fluid superficial velocity (adapted from [20][37])

For each simulation the superficial, minimum fluidization and terminal velocities were calculated. With the u_{mf} and u_t a linear relationship between the bed porosity and the superficial velocity was found. The bed porosity is then calculated with this new found equation, using the superficial velocity.

The superficial velocity (u) is obtained in the usual manner (m.s⁻¹):

$$u = \frac{Q_v}{A_s} \quad (3.23)$$

Where Q_v represents the volumetric flow and A_s the reactor's cross area.

3.1.4. Particle Size Distribution

Soares model [26] was developed for CSTR. However, one of the main assumptions in this work is that the RTD of the solids for the considered FBR is approximated to the one of a CSTR. The model equations developed by Soares [26] remain applicable.

The following assumptions were made when developing this model:

- All active sites on the catalyst have the same propagation constant;
- The concentration of active sites is uniform throughout the catalyst and polymer particles;
- The catalyst possesses only stable active sites that do not suffer deactivation;
- The catalyst particle shape is considered to be a sphere;

Nowadays it is known that Ziegler-Natta catalysts have more than one type of active sites, each with its characteristic kinetic rate propagation constant, chain transfer and deactivation. These different types of active sites are the main reason for the broad molecular weight and chemical composition distributions. In this model, however, it is sufficient to employ an average propagation constant because only particle growth is of interest.

The second assumption is supported by the fact that good replication would not occur unless the active sites are uniformly distributed on the catalyst particle.

The third assumption, while less realistic, is made to simplify the model while also allowing to obtain significant conclusions regarding the model's objective, which is to analyze the effect of polymer swelling on the PSD.

The particle size can be obtain using equation (3.24) [26]:

$$d_p = d_c (1 + \alpha t)^{1/3} \quad (3.24)$$

Correspondent to this particle size, there is a particle population given by equation (3.25) [26].

$$F(d_p) = \frac{3(1 + \alpha t)^{1/3} e^{-t/\tau}}{\alpha D_c \tau} \quad (3.25)$$

Wherein,

$$\alpha = \frac{k_p C_{Et}^P C^* MW_{Et}}{\rho_{pol}} \quad (3.26)$$

Where D_p is the diameter (cm) of the polymer particle, D_c is the diameter of the catalyst particle (cm), t is the reaction time (min), τ is the average residence time of the reactor (min) and α is a combined kinetic parameter (min^{-1}). In equation (3.26) k_{prop} is the average propagation constant ($\text{cm}^3 \cdot \text{mol}^{-1} \cdot \text{min}^{-1}$), C_{Et}^P is the monomer concentration in the polymer phase (at the active sites) ($\text{mol} \cdot \text{cm}^{-3}$), C^* is the active sites concentration in the catalyst ($\text{mol} \cdot \text{cm}^{-3}$), MW_{Et} is the molar mass of the monomer ($\text{g} \cdot \text{mol}^{-1}$) and ρ_{pol} is the specific weight of the obtained polymer ($\text{g} \cdot \text{cm}^{-3}$).

However, the main limitation of the model, is that it was developed for one catalyst particle, while in reality the catalyst presents its own PSD. As such, an algorithm was developed to discretize the PSD and include this important contribution.

The algorithm starts with the establishment of small intervals to categorize the polymer particles. Then, for each catalyst size, the polymer particle size is compared to the intervals frontiers to decide if it fits in that interval. If it does, then the population in that interval increases, but not before it is affected with the volume fraction corresponding to its original inlet catalyst. This allows for a more comprehensive view of the particle size distribution of the polymer that is being produced, by simulating a catalyst feed with different particle sizes.

From the particle size distribution, it is also possible to obtain the most common particle size of the polymer phase, which is considered to be particle diameter (d_p) for all calculations. For this step, an algorithm was developed that compares the population of each interval and selects the one with the largest population.

3.2. Model Implementation

The model was implemented using *Matlab*®. For the development of the code, there were two main concerns: The need to use a solver that allows a set of non-linear equations and the need to iterate the mean particle size (d_p), since the mean diameter of the particles is obtained from the polymer PSD, which is computed after the reactor equations.

To solve the reactor equations, *Matlab*'s Optimization Toolbox's *fsolve* function was used. This function requires a matrix with the initial guess for every variable, since all the equations are solved simultaneously. Consequently, an auxiliary and simplified version of the model was developed in *Microsoft Excel*® to obtain the required initial values. This shortened *Excel* model doesn't account for catalyst or polymer PSD and operates under the initial assumption of solids temperature (T_s). The model equations are introduced leading to the heat balance where T_s is calculated rearranging equation (3.18).

To assemble the model an iterative cycle is proposed, as seen in Figure 3.2. For each ICA partial pressure and for each catalyst size, the reactor and PSD models are run, returning a mean particle size (d_p). This value is then compared to the initial mean particle size, to ensure that the model converges. For that, the *deviation* variable is defined as the difference between the initial and final mean particle sizes. In order for the cycle to conclude, the deviation must be

lower than a fixed *error*, chosen by the user. If the loop of the cycle is done without converging and preparing to re-run, the initial particle size is substituted for the most recently computed mean particle size. Once the mean particle size converges, the cycle moves on to the next catalyst size. Just as all the catalyst sizes were run, the model adds up the polymer PSD for each catalyst size and makes the necessary calculations for the average reactor properties, such as bulk and solids temperature, PE production rate, pressure drop and all other relevant output parameters. To average these properties and parameters, they are multiplied by the volume fraction of the catalyst it pertains. For a hypothetical property, Z , this calculation would take the following form:

$$\bar{Z} = \sum Z_n \cdot F(d_c)_n \quad (3.27)$$

Where \bar{Z} is the averaged Z property, Z_n is the Z property when calculated with the n size catalyst, and $F(d_c)_n$ is the volume fraction of the n size catalyst.

Once the PSD's are added, the cycle moves on to the next ICA partial pressure. When the model runs all the ICA partial pressure the cycle is complete.

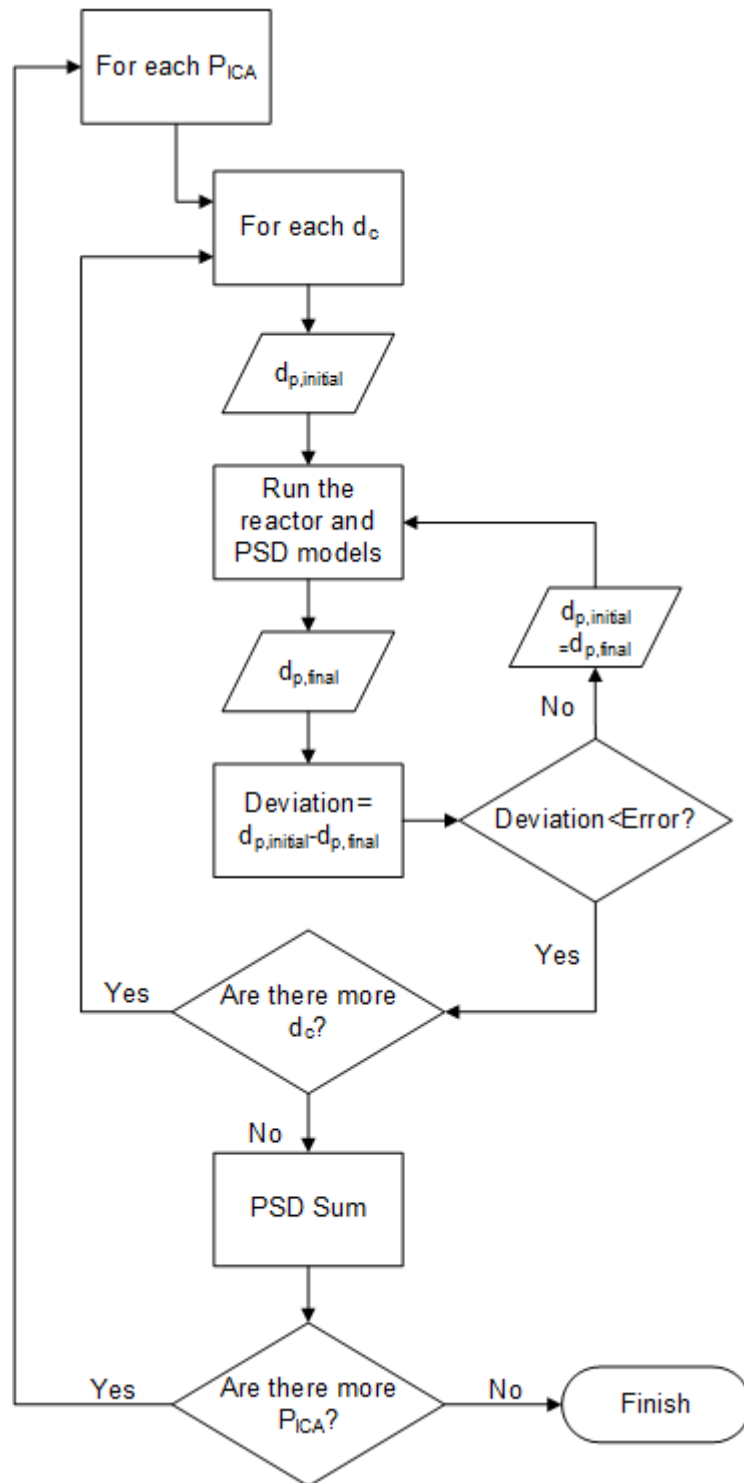


Figure 3.2. Main iterative cycle flowchart.

4. Results

In this chapter the results of the simulations ran are presented and discussed.

The common parameters used in all simulations are summarized in Table 4.1. The properties of the gas phase calculations were based on [38][39] and are presented in Appendix B.

Table 4.1. Properties of the solid phase, reaction parameters and reactor properties.

Parameter	Units	Value	Reference
Reactor Diameter, d	m	4.75	[40]
Reactor Bed Height, h_b	m	13.3	[40]
Catalyst type	-	Ziegler Natta	[41]
Catalyst Particle Diameter, d_c	μm	49; 55; 63	[41]
Initial Catalyst Active Site Concentration, C_0^*	mol/m^3_c	0.52	[41]
Catalyst Density, ρ_c	kg/m^3	2300	[41]
Catalyst Heat Capacity, $C_{p,c}$	$\text{J}/(\text{kg}\cdot\text{K})$	2000	[41]
Polymer Heat Capacity, $C_{p,p}$	$\text{J}/(\text{kg}\cdot\text{K})$	2000	[41]
Kinetic rate constant, $k_p^{80^\circ\text{C}}$	$\text{m}^3/(\text{mol}\cdot\text{s})$	180	[41]
Kinetic propagation constant, k_{prop}	$\text{m}^3/(\text{mol}\cdot\text{min})$	1.87×10^{10}	[41]
Catalyst deactivation rate constant, $k_d^{80^\circ\text{C}}$	s^{-1}	1×10^{-4}	[41]
Reaction Activation Energy, E_a	J/mol	42000	[41]
Catalyst Deactivation Energy, E_d	J/mol	42000	[41]
Heat of Reaction, ΔH_{pol}	J/mol	-107600	[41]
Minimum Fluidized Bed Porosity, $\epsilon_{m.f.}$	-	0.476	[20]
Reference Temperature T_{ref}	K	80	-

In all simulations three catalyst particle sizes were used, following the distribution presented below:

Catalyst Particle Diameter d_c (μm)	Volumetric fraction
49	0.3037
55	0.3391
63	0.3572

4.1. ICA effect on ethylene solubility and polymer density

To better understand the effects on the ICA on reactor behavior, it is first necessary to understand the effects that the presence of these alkanes have on ethylene concentration in polymer phase and amorphous polymer density. All information regarding these calculations is presented in Appendix A.

Using the SL-EoS based solubility and polymer phase density, concentration of each gaseous component in the polymer phase in ternary systems were calculated and the results are shown in Figure 4.1.

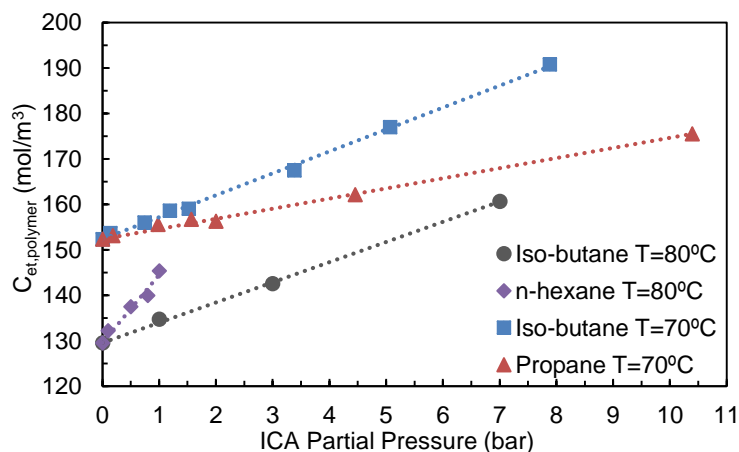


Figure 4.1 ICA effect on the concentration of ethylene in the polymer phase at 70° C and 80° C obtained from the SL-EoS in ternary (ethylene(1)/ICA(2)/PE(1)) systems

The increase in the ICA partial pressure in the gas phase leads to the increase of ethylene concentration in the polymer phase. In addition, the higher the carbon number of the ICA the higher is the ethylene concentration in the polymer phase at the same conditions. This observation can be attributed to the co-solvent effect of alkanes on the solubility of ethylene which manifest itself in multicomponent gases/polymer systems and is well known in the open literature. An increase in temperature leads to lower ethylene solubility in the polymer phase.

Figure 4.2 shows the effect of ethylene/ICA mixtures on the polymer densities ternary systems estimated by the SL-EoS. It can be noticed that the higher the carbon number of the ICA the lower is the polymer phase density at given conditions which is in agreement with the discussion made above.

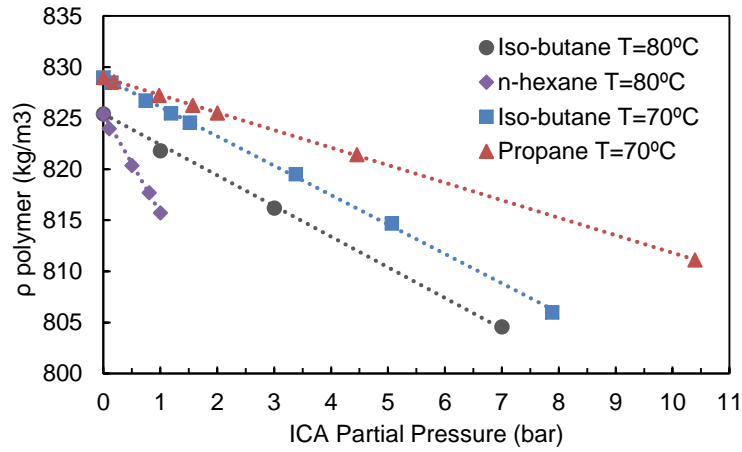


Figure 4.2. ICA effect on polymer density at 70°C and 80°C obtained from the SL-EoS in ternary (ethylene(1)/ICA(2)/PE(1)) systems.

For the ease of calculations, correlations were developed for the ethylene and ICA concentration in the polymer phase (C_{Et}^P and C_{ICA}^P) and the polymer density, as shown by the fitted lines in Figure 4.1 and 4.2. These correlations took the following form:

$$C_{Et}^P = A \cdot P_{ICA} + B \quad (4.1)$$

$$C_{ICA}^P = C \cdot P_{ICA} \quad (4.2)$$

$$\rho_{polymer} = -D \cdot P_{ICA} + E \quad (4.3)$$

Table 4.2. Coefficients for the correlations of ethylene and ICA concentration on polymer phase (mol.m^{-3}) and polymer density (kg.m^{-3}).

	70°C		80°C	
	Propane	Iso-butane	Iso-butane	n-hexane
A	2.16	4.82	4.84	13.71
B	152.35	152.35	129.5	129.5
C	75.25	237.69	120.38	343.50
D	1.71	2.87	3.26	9.11
E	828.97	828.97	825.90	825.90

4.2. Model Validation

The model validation was carried out by replicating the example 7C of the patent US 6,864,332 B2 [40]. The data used is shown in table 4.3.

Table 4.3. Data used in the validation of the model (adapted from [40])

Reactor Abs. Pressure (bar)	22.4
Inlet Temperature (°C)	35
Inlet gas flowrate (kg/s)	335
Inlet Catalyst flowrate (kg/s)	0.0024
Ethylene Partial Pressure (bar)	7.8
Propane Partial Pressure (bar)	4.3
Iso-butane Partial Pressure (bar)	3.3

Since in the example there are two ICA, some minor alterations were made to the reactor equations. All equations regarding the ICA are still written in the same fashion, but accounting for two ICA compounds instead of one.

For the ethylene concentration in the polymer (C_{Et}^P), a blunt approximation was made. Since the SL-EoS code was extended only for ternary systems in order to estimate the concentrations and polymer phase density, there is no possible way to obtain from the model the values for the propane/iso-butane/ethylene/PE system. Consequently, C_{Et}^P is estimated using a combination of the equations obtained for each of the separate ICA. The solubility of ICA in the polymer was considered to not be affected by the presence of another ICA. Further information on this approximation is available in appendix A.

The following Table 4.4 shows the comparison between the results presented in example 7C [40] and the results obtained in the simulation.

Table 4.4 – Comparison between the results presented in example 7C [40] and the simulation (Sim.) and the corresponding variation (Δ).

	Example 7C	Simulation	Δ (%)
PE Production Rate (ton/h)	28.9	30.1	4.2
Reactor Temperature (°C)	88	88	0.0
Superficial Velocity (m/s)	0.75	0.75	0.0

Analyzing the results presented it is evident that the developed model is a good approximation of reality. The slight difference in the polyethylene production rate can be explained by use of a different catalyst and due to the solubility values only availability at 70°C and 80°C for iso-butane and at 70°C for propane and the reactor operates at 88°C. The increase in reactor temperature leads to a decrease in solubility and, therefore a decrease in ethylene concentration in the polymer phase. Equation (3.7) shows that reduced ethylene concentration leads to lower reaction rates. Furthermore, it has never been investigated in the open literature via sorption-dilatation experiments that if there are two alkanes in the gas phase along with an olefin, then how

do co-solubility effects manifest themselves. Based on the current results and available information, the model can be considered reasonably valid.

4.3. Simulation I

To evaluate the influence of increasing the ICA partial pressure in reactor behavior and polymer PSD, several simulations were run. The initial simulation considered a fixed inlet catalyst and gas flow and aim to disclose how the presence of ICA affects the reactor's parameters, such as temperature, rate of production, ethylene conversion and product PSD. Table 4.5 summarizes the used values. Nitrogen was used to achieve the desired reactor pressure and keep it constant throughout the simulations.

Since the model was developed for dry mode, the maximum partial pressure of the ICA is dependent on the inlet temperature, to ensure that no liquids are present in the stream. The values of the partial pressure were also chosen to ensure that the reactors temperature is the range around 70°C, since the solubility data is only available at this temperature.

Table 4.5. Simulation I reactor parameters.

Reactor Abs. Pressure (bar)	20
Inlet Temperature (°C)	35
Inlet gas flowrate (mol/s)	10000
Inlet Catalyst flowrate (kg/s)	0.0011
Ethylene Partial Pressure (bar)	7
Propane Partial Pressure (bar)	0 to 7
Iso-butane Partial Pressure (bar)	0 to 4

The results for simulation I are presented in Figures 4.3 to 4.6.

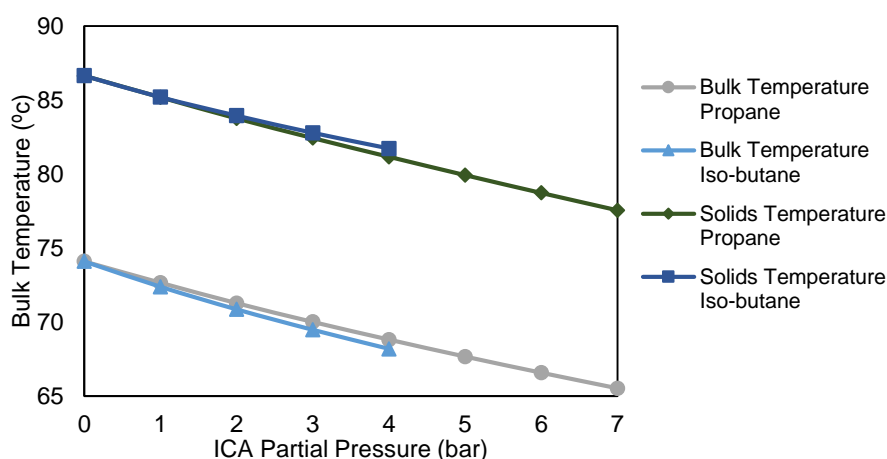


Figure 4.3. Effect of ICA on reactor bulk and solids temperature for simulation I.

As it is expected, the temperature decreases with the increase of ICA. This is due to the ICA increasing the global specific heat of the gas-phase. It is possible to observe that for the same pressures, iso-butane has a slightly higher cooling effect. This happens because specific heat of iso-butane is higher than the specific heat of propane.

It is also interesting to observe that although the bulk temperature of the reactor when using iso-butane is lower than when using propane, the solids temperature is higher when compared to the propane simulation. This can be explained by the more pronounced co-solubility effect that iso-butane has in the system. The bigger the effect of co-solubility, the higher ethylene concentration in the polymer phase. That leads to higher PE production rates, which releases more heat of reaction. Figure 4.4. shows the effect of ICA in the PE production rate.

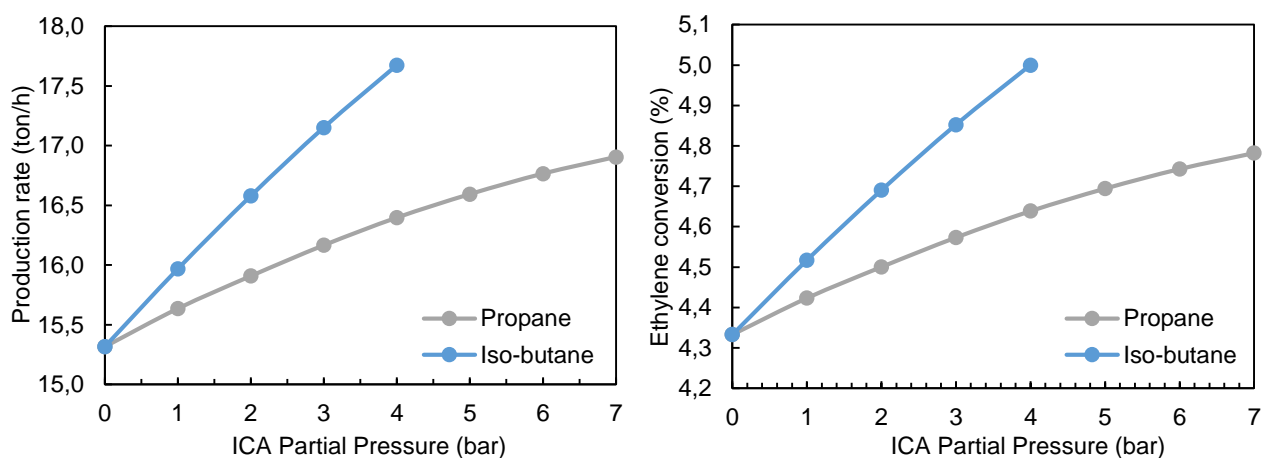


Figure 4.4. Effect of ICA on: (a) PE Production rate and (b) Ethylene per pass conversion. Values regarding simulation I.

Figure 4.4 allows to conclude that the production rate, and consequently the ethylene conversion, increase with the presence of more ICA, which consolidates the results shown in Figure 4.3.

It is interesting to observe the different shapes of the curves. This is a result of the different effect that iso-butane and propane have on the ethylene solubility in the polymer phase. Iso-butane is a bigger molecule and induces a higher co-solubility effect than propane.

In terms of production rate, using 4 bar of propane leads to a 7% increase. Contrasting with this value, the same amount of iso-butane leads to a 15% increase. In fact, even when using 7 bar of propane, the production is still lower than when using 4 bar of iso-butane. This is again a direct consequence of the co-solubility effect.

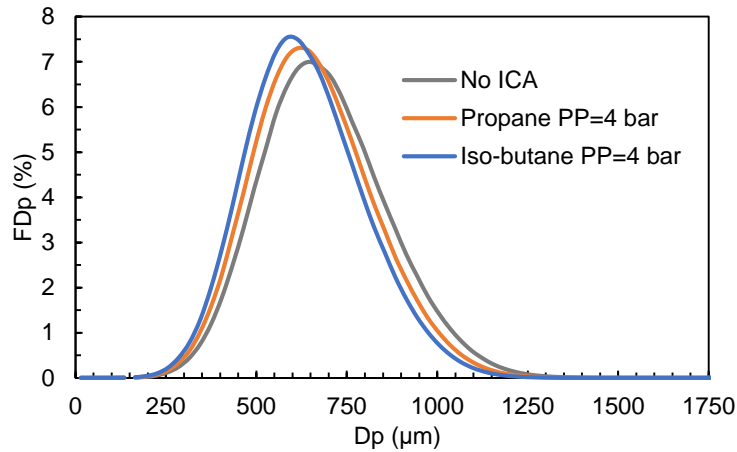


Figure 4.5. Effect of ICA on polymer PSD for simulation I.

In this simulation the mean particle size of the polymer decreases with the increase of ICA. This is a consequence of the solids temperature decrease, a highly important parameter in the PSD algorithm. In fact, an increase in the mean particle size could also be expected. Analyzing the PSD equations (3.24) to (3.26), it is easy to assume that the increase in ICA partial pressure would lead to bigger particle sizes. However, the rise in ICA partial pressure and consequent increase in ethylene solubility in the polymer phase are proven to have a less significant effect than the solids temperature in the polymer PSD model. This can also be seen in section 4.6 Simulation IV (Figure 4.17).

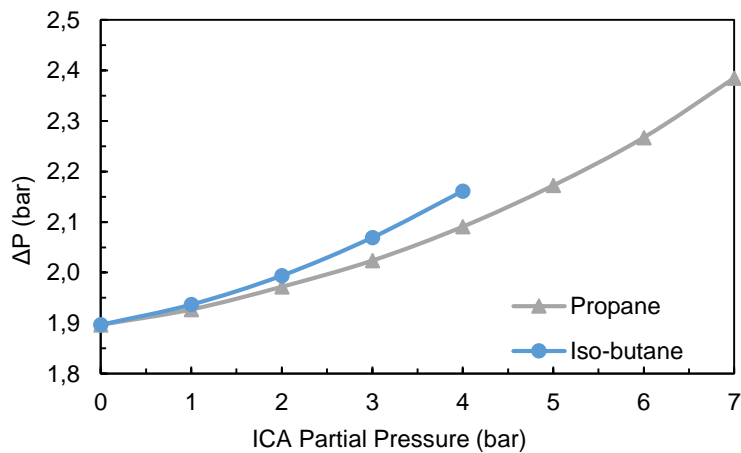


Figure 4.6. Effect of ICA on reactor pressure drop for simulation I.

The pressure drop in the reactor increases with the increase of ICA present. This is an expected behavior. Equation (3.20) shows that the decrease of particle size will lead to the increase of pressure drop. As seen from Figure 4.5 the mean particle size decreases with the increase of ICA, leading to a higher pressure drop.

Both the superficial velocity and bed porosity maintained constant values regardless of the ICA pressure and alkane used. The simulation presents a bed porosity of 0.6 and a superficial velocity of 0.8 m/s. All the values retrieved from this simulation are presented in Appendix C.

4.4. Simulation II

Simulation II compares the effects of ICA in the ranges of 70°C and 80°C in order to understand in which reactor parameters the temperature effects overtake the increase/decrease of ethylene concentration in polymer phase and vice-versa. The values used are summarized in table 4.6.

Table 4.6 - Simulation II reactor parameters.

	70°C	80°C
Reactor Abs. Pressure (bar)	20	20
Inlet Temperature (°C)	35	35
Inlet gas flowrate (mol/s)	10000	10000
Inlet Catalyst flowrate (kg/s)	0.0011	0.0016
Ethylene Partial Pressure (bar)	7	7
Iso-butane Partial Pressure (bar)	0 to 4	0 to 4

The results are displayed in Figures 4.7 and 4.8.

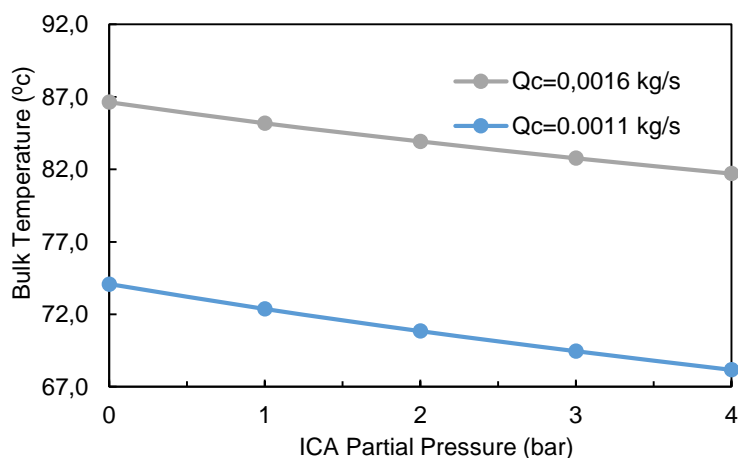


Figure 4.7. Effect of ICA on reactor temperature for simulation II.

The increase in catalyst inlet flowrate allows to increase the reaction temperature so that there are two separate temperature ranges: one around 80°C and another around 70°C. The curves represented in Figure 4.7 can be interpreted in the same fashion as the ones presented in Figure 4.3. The temperature decreases with the presence of ICA in both temperature ranges, due to the cooling effect that the alkane introduces.

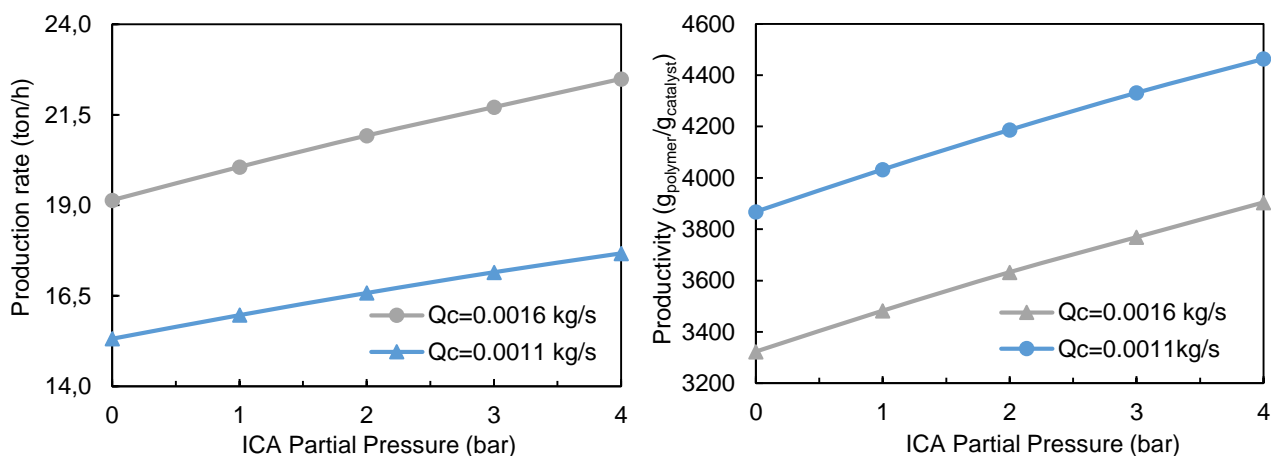


Figure 4.8. Effect of ICA on: (a) PE Production rate and (b) productivity. Values regarding simulation

II.

The increase in the catalyst inlet flowrate leads to higher production rates (Figure 4.8(a)). However, the productivity lowers when more catalyst is used, since the increase in temperature results in a decrease in ethylene solubility (see Figure 4.1.). Figure 4.8(b) also shows another interesting behavior: regarding the catalyst productivity, the effect of the temperature is outweighed by the effect of the ethylene concentration present in the polymer phase

Other reactor parameters also don't show sensitivity to the temperature changes. All the values from this simulation are presented in Appendix C.

4.5. Simulation III

Simulation III consist of keeping the reactor production rate and temperature constant while varying the partial pressure of ICA. This allows to understand better the implications of adding ICA into a current process, since the production rate might need to be kept in the existing facility. The values used in this simulation are presented in table below.

Table 4.7 - Simulation III reactor parameters.

Reactor Abs. Pressure (bar)	20
Inlet Temperature (°C)	35
Reactor temperature (°C)	70
PE Production rate (ton/h)	15.8
Ethylene Partial Pressure (bar)	7
Propane Partial Pressure (bar)	0 to 9
Iso-butane Partial Pressure (bar)	0 to 4

The results for this simulation are presented in figures 4.9 to 4.12.

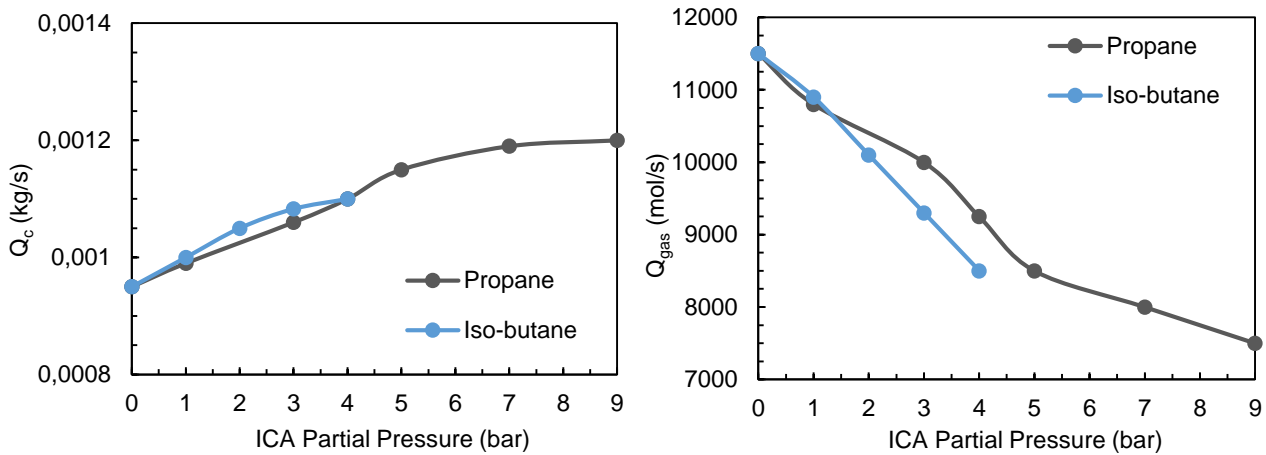


Figure 4.9. Effect of ICA on: (a) Catalyst inlet flowrate and (b) gas inlet flowrate. Values regarding simulation III.

The results obtained are expected. Since the ICA has a cooling effect in the reactor (see Figure 4.3), it is necessary to decrease the inlet gas flowrate to maintain the temperature at 70°C. However, a decrease in the inlet flowrate leads to a decrease in production. Therefore, it is also necessary to increase the catalyst feed.

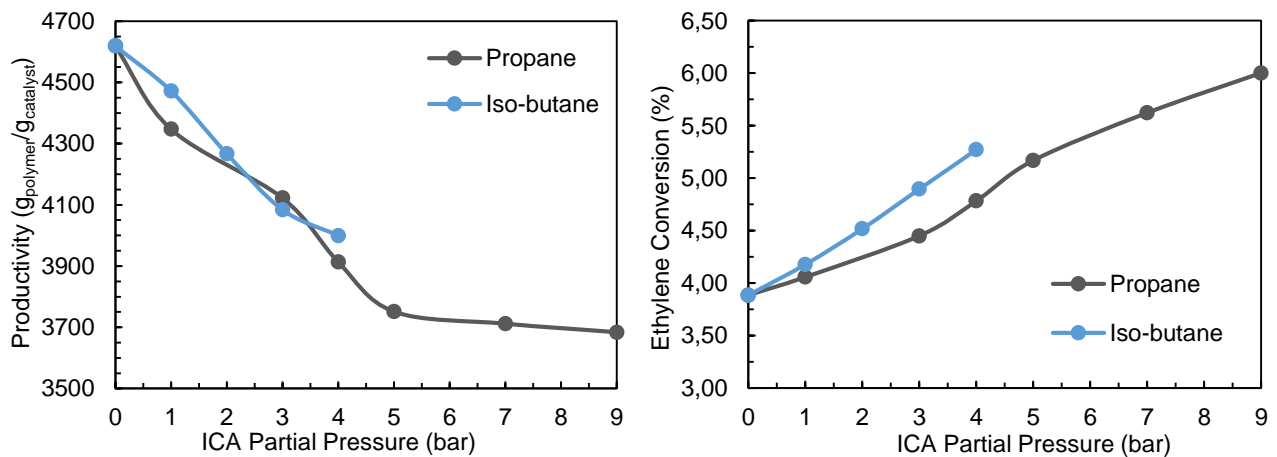


Figure 4.10. Effect of ICA on: (a) Productivity and (b) ethylene per pass conversion. Values regarding simulation III.

The productivity of the catalyst decreases with the increase of the ICA partial pressure, but not because of the change in the ICA partial pressure. The decrease in catalyst productivity is related to the decrease of the inlet gas flowrate, which leads to less ethylene being available. The same amount of PE is being produced, but a higher amount of catalyst is necessary to guarantee the production rate. The ethylene conversion is increasing, since a constant amount of PE is being produced, but the inlet flow of ethylene is decreasing.

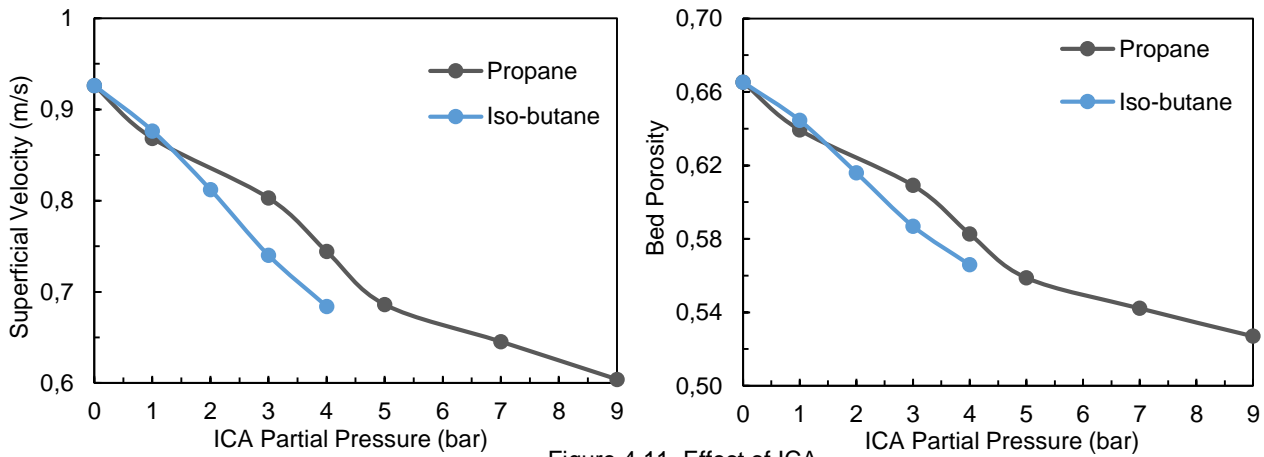


Figure 4.11. Effect of ICA

on: (a) Superficial velocity and (b) bed porosity. Values regarding simulation III.

The decrease in superficial velocity, due to the change in gas inlet flowrate leads to a contraction of the bed. Even though there is a major decrease in gas inlet flowrate, the conditions still ensure full bed fluidization. Targeting the simulation with propane at 9 bar (lowest inlet gas flowrate), we can observe that the bed porosity remains well above the minimum fluidization porosity of 0,476. From Table 4.8. it is possible to observe that the superficial velocity is kept between the minimum fluidization velocity and the terminal velocity for the mean particle size.

Table 4.8. Summary of the minimum fluidization, superficial and terminal velocities for the average particle size in the reactor. Values regarding simulation III.

	ICA Partial Pressure (bar)	Minimum fluidization velocity (m/s)	Superficial velocity (m/s)	Terminal velocity (m/s)
Iso-butane	4	0.29	0.68	4.07
Propane	9	0.37	0.60	5.03

Figure 4.12 shows the results for the polymer PSD.

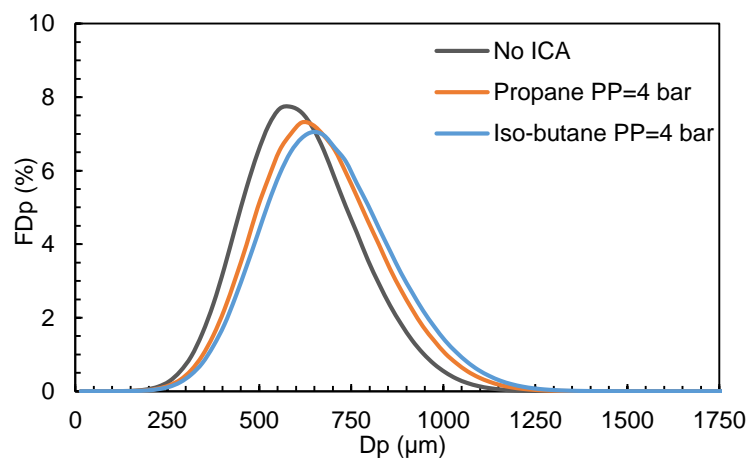


Figure 4.12. Effect of the ICA on polymer PDS for simulation III.

Analyzing Figure 4.12 it clear that the mean particle size increases with the presence of more ICA, contrasting Figure 4.5. Since the temperature is kept constant it is possible to observe the co-solubility effects, which lead to higher ethylene concentration in the polymer phase.

4.6. Simulation IV

Simulation IV allows to observe the effect of the ICA on the polymer PSD, since the simulations were ran using only the PSD model, keeping ethylene concentration and bulk temperature fixed.

When the temperature is kept constant at 80°C, the ICA's used are n-hexane (partial pressure between 0-1 bar) and iso-butane (partial pressure between 0-4 bar).

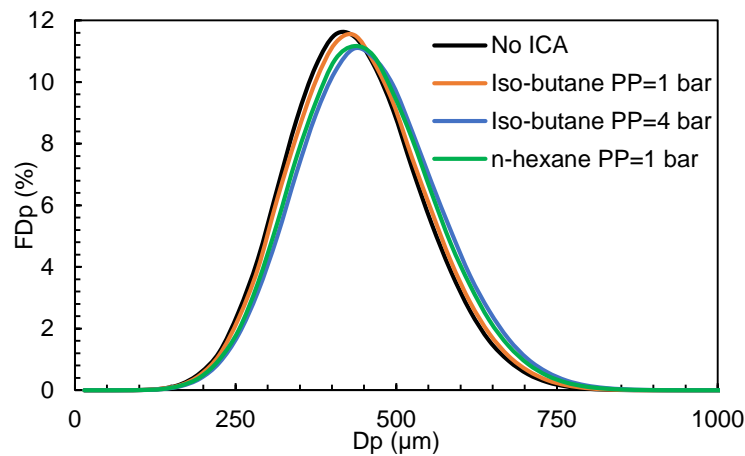


Figure 4.13. Effect of ICA on the polymer PSD at 80°C

The difference caused by the ICA in the PSD is not very striking. It is clear that the increase of ICA leads to bigger particles. However, when zooming in at the top of curves (Figure 4.14) it is possible to observe the influence of the different ICA's.

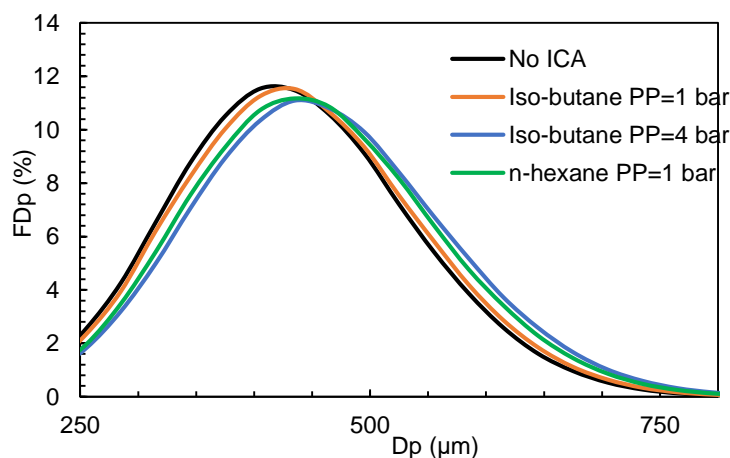


Figure 4.14. Effect of ICA on polymer PSD at 80°C (zoomed).

It becomes obvious that the heavier alkane (n-hexane) is responsible for a much higher increase in the average particle size than the lighter alkane (iso-butane). This difference is so

pronounced that to get similar PSD where the mean particle size increases 7% one must use 1 bar of n-hexane or 4 bar of iso-butane. This is a direct effect of co-solubility phenomena. The following Table shows the average particle sizes for each ICA.

Table 4.9. Average particle size for iso-butane and n-hexane at 80°C.

	Partial pressure (bar)	Average particle size (μm)
No ICA	-	380
iso-butane	1	400
iso-butane	4	430
n-hexane	1	430

For a constant temperature of 70°C the ICA's used are iso-butane (partial pressure between 0-4 bar) and propane (partial pressure between 0-10 bar).

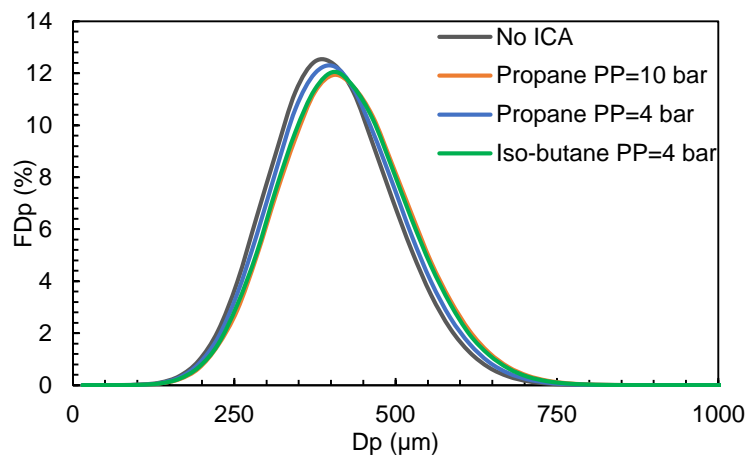


Figure 4.15. Effect of ICA on polymer PSD at 70°C.

Like in Figure 4.13, the effect of the ICA on the polymer PSD is minimal. However, it is again interesting to observe the top of the curves (Figure 4.16)

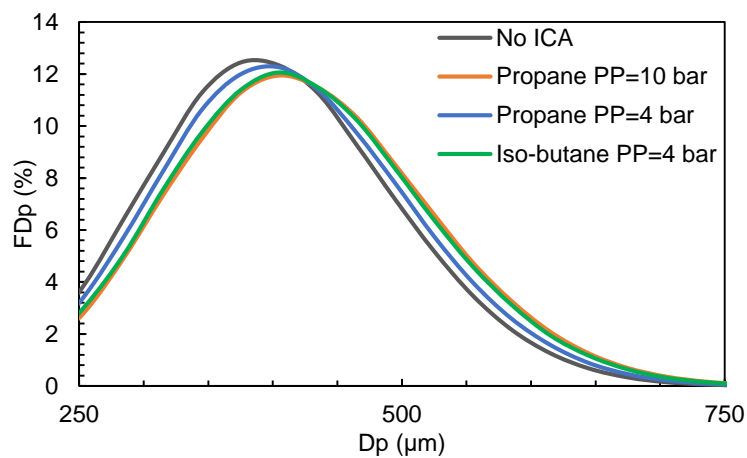


Figure 4.16. Effect of ICA on polymer PSD at 70°C (zoomed).

Iso-butane is now the heavier alkane and when the partial pressure is 4 bar the PSD is similar to the PSD of propane at a partial pressure of 10 bar. The following Table shows the average particle sizes for each ICA.

Table 4.10. Average particle size for propane and iso-butane at 70°C

	Partial pressure (bar)	Average particle size (µm)
No ICA	-	385
iso-butane	4	408
Propane	4	400
Propane	10	408

To further investigate about the temperature effect, Figure 4.17 shows a comparison of the polymer PDS using iso-butane at a partial pressure of 4 bar at 70°C and 80°C.

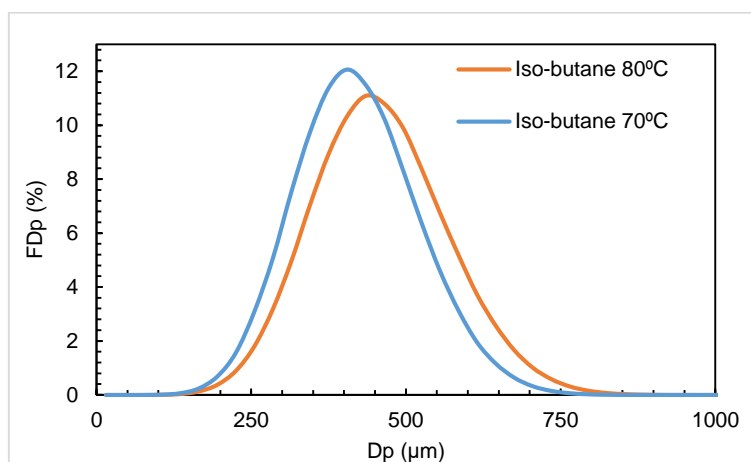


Figure 4.17. Effect of temperature in polymer PDS for iso-butane (partial pressure 4 bar).

Figure 4.17 shows that the temperature is a parameter of much higher importance in the polymer PSD. Even though at 70°C the concentration of ethylene in the polymer phase is higher than at 80°C, the polymer still exhibits smaller particles. The average particle size increases 5% when the temperature is increased by 10 °C.

4.7. Sensitivity Analysis

A sensitivity analysis was conducted in order to determine the parameters that most influence the model outputs. In this section four parameters analysis will be presented and discussed.

The data assumed for the simulation will be the one considered in simulation I, using only iso-butane with a partial pressure of 2 bar. The parameters discussed here will be:

- Catalyst activity, varying the kinetic rate constant $k_p^{T_{ref}}$;
- Ethylene concentration in amorphous polymer phase, C_{Et}^p ;

- Alkane partial pressure, P_{ICA} ;
- Inlet flow temperature, T_0 .

The catalyst activity is an important parameter to analyze. Not only is catalyst activity directly related to HDPE production but it is also related to the reactor and solids temperature due to the change in polymerization heat released. Catalyst activity may vary depending on the type of catalyst used, so variations of ± 10 and ± 30 % to $k_p^{T_{ref}}$ were considered.

Ethylene solubility in the growing polymer phase is, as discussed before, one of the most important parameters in the kinetic equations. It defines the effective concentration of monomer that is available near the catalyst active sites for polymerization. Variations of ± 10 and ± 20 % were considered to C_{Et}^p .

Another parameter to analyze will be the alkane partial pressure, in this case iso-butane. Considering the objectives of this work this as crucial parameter. The quantity of iso-butane present in the reactor has effect on heat absorption, ethylene solubility in HDPE and, therefore, polymer production, productivity and conversion. Variations of $\pm 40\%$ and ± 80 % were considered.

The final analyzed parameter will be the inlet flow temperature T_0 . It is interesting to observe how a difference in the temperature of the inlet stream will affect the production and temperature of the reactor, especially considering that the inlet temperature was maintained constant throughout simulation I to simulation III. Variations of ± 10 % and ± 30 % will be considered.

4.7.1. Catalyst activity

Table 4.11. showcases the results for the sensitivity analysis of the catalyst activity, in which the kinetic rate constant was varied.

Table 4.11. Sensitivity analysis results for the variation of $k_p^{T_{ref}}$ ($m^3 \cdot mol^{-1} \cdot s^{-1}$)

Variation	Parameter Varied: $k_p^{T_{ref}}$			
	10%	30%	-10%	-30%
Δ Temperature bulk (%)	4,1	11,8	-4,3	-13,8
Δ Pressure drop (%)	9,1	31,2	-8,0	-20,9
Δ Per pass conversion (%)	8,5	24,7	-8,8	-28,0
Δ Productivity (%)	8,5	24,7	-8,8	-28,0
Δ Production Rate (%)	8,5	24,7	-8,8	-28,0
Δ Bed Porosity (%)	-1,7	-4,8	1,7	5,2
Δ Mean Particle Size (%)	4,5	13,9	-4,1	-11,5

Analyzing the results resumed in Table 4.11 it is possible to conclude that the catalyst activity affects, as expected, the model outputs significantly.

A variation of +10% in $k_p^{T_{ref}}$ produces an increase of 8,5% in production rate, productivity and ethylene per conversion. This is an expected occurrence since the production rate, productivity and ethylene per conversion are directly to the rate reaction equation (3.7), which depends on $k_p^{T_s}$. This parameter is obtained by using an Arrhenius Law with dependence on temperature, that relies on $k_p^{T_{ref}}$ value.

When a 10% variation in $k_p^{T_{ref}}$ occurs, a 4,1% variation in bulk temperature is observed. This is essentially related to the increase in polyethylene production. With higher production there is a higher amount of polymerization heat being released but since here there is no exponential dependence of the heat balance parameters on temperature, the observed variation in bulk temperature is lower than the one observed in production.

A variation of +10% in $k_p^{T_{ref}}$ leads to a 9,1% increase of the pressure drop. This value is justified by the fact that the pressure drop has a quadratic dependence on the particle size, which has increased 4,5% (due to the temperature increase).

When changing the value variation from + 10% to + 30 % the variations of the output parameters changes three fold, expectedly. Negative variations (-10 and -50 %), however, appear to have a stronger effect on the output parameters. This is due to the fact that the developed model is not linear.

4.7.2. Ethylene concentration in amorphous polymer phase

Table 4.12 shows the results for the sensitivity analysis of the ethylene concentration in amorphous polymer phase.

Table 4.12. Sensitivity analysis results for the variation of ethylene concentration in polymer phase (C_{Et}^p) (mol.m⁻³)

Variation	Parameter Varied: C_{Et}^p			
	10%	30%	-10%	-20%
Δ Temperature bulk (%)	2,3	7,1	-2,0	-3,6
Δ Pressure drop (%)	18,0	65,4	-15,3	-28,4
Δ Per pass conversion (%)	4,8	14,9	-4,2	-7,4
Δ Productivity (%)	4,8	14,9	-4,2	-7,4
Δ Production Rate (%)	4,8	14,9	-4,2	-7,4
Δ Bed Porosity (%)	-3,2	-8,5	3,9	8,8
Δ Mean Particle Size (%)	7,8	24,5	-7,4	-14,7

A variation of +10% in C_{Et}^p produces an increase of 4,8% in production rate, productivity and ethylene per conversion. Like mention previously, this is an expected behavior since the production rate, productivity and ethylene per conversion are directly to the rate reaction equation (3.7), which depends also depends on C_{Et}^p .

When 10% variation in C_{Et}^p occurs, a 2,3% variation bulk temperature is observed. Like before, this is essentially related to the increase in production.

A variation of +10% in C_{Et}^p leads to a 18% increase of the pressure drop. This value is justified by the fact that the pressure drop has a quadratic dependence on the particle size, which has increased 7,8%. The increase in mean particle size is a combination of two different effects: the increase in temperature and the direct increase in C_{Et}^p , which affects the particle size prediction (see equations (3.24) and (3.26)).

Observing table 4.12 it is possible to conclude the changing the value variation from + 10% to + 30 % the variations of the output parameters also three fold. Negative variations (-10 and -20 %) still have a stronger effect on the output parameters.

4.7.3. ICA partial pressure

Table 4.13 shows the results of the sensitivity analysis for the variation of iso-butane partial pressure.

Table 4.13. Sensitivity analysis results for the variation of iso-butane partial pressure (P_{ICA}) (bar)

Parameter Varied: P_{ICA}				
Variation	40%	80%	-40%	-80%
Δ Temperature bulk (%)	-1,6	-3,1	1,7	3,5
Δ Pressure drop (%)	3,0	6,5	-2,3	-4,1
Δ Per pass conversion (%)	2,7	5,4	-2,9	-6,1
Δ Productivity (%)	2,7	5,4	-2,9	-6,1
Δ Production Rate (%)	2,7	5,4	-2,9	-6,1
Δ Bed Porosity (%)	0,2	0,4	-0,4	-0,9
Δ Mean Particle Size (%)	-1,3	-2,5	1,6	3,5

Table 4.13 shows that a variation in P_{ICA} causes a difference in the model outputs. This is due to the difference in ethylene solubility that increases with the higher amount of iso-butane present in the reactor (co-solubility effect).

A 1,6% variation in the bulk temperature is observed when 40% variation in P_{ICA} occurs. This is related to the production increase, but also to the changes that the presence of iso-butane induces in the gas heat capacity.

Changing the value variation from + 40% to + 80 % the variations of the output parameters duplicate. Negative variations (-40 and -80 %) continue to have a stronger effect on the output parameters.

4.7.4. Inlet Temperature

Table 4.14 shows the results of the sensitivity analysis of the inlet temperature.

Table 4.14. Sensitivity analysis results for the variation of the inlet temperature (T_0) (K)

Variation	Parameter Varied: T_0			
	10%	30%	-10%	-20%
Δ Temperature bulk (%)	2,9	9,4	-2,6	-7,0
Δ Pressure drop (%)	11,9	42,4	-10,1	-25,5
Δ Per pass conversion (%)	-3,5	-9,2	4,0	13,7
Δ Productivity (%)	-3,5	-9,2	4,0	13,7
Δ Production Rate (%)	-3,5	-9,2	4,0	13,7
Δ Bed Porosity (%)	-2,3	-6,5	2,5	7,7
Δ Mean Particle Size (%)	5,1	16,3	-4,6	-12,5

The results from Table 4.14 show a considerable effect of inlet flow temperature in the model outputs. The decrease/increase in production rate, per pass conversion and productivity shown when decreasing/increasing the inlet flow temperature T_0 is once again related to the CSTR approach. A higher inlet temperature results in higher temperature increase within the reactor, which increases the rate of polymerization. The increase/decrease in mean particle size can again be explained by the increase/decrease in temperature. The variations in the mean particle size are once more responsible for the changes observed in pressure drop.

5. Conclusions

The present model refers to gas-phase fluidized bed reactor, the most used in industrial polyethylene production. The model inputs are the catalyst PSD, inlet temperature, total and partial pressures, inlet flowrates, as well as other reactor specifications (diameter, bed height, etc.). It predicts the polymer production, bulk and solids temperatures, polymer PSD, mean particle size and bed porosity as the main calculated variables. In addition, it also predicts catalyst activity, ethylene per pass conversion, minimum fluidization velocity, superficial velocity, terminal velocity and pressure drop. The model was implemented based on the assumption of dry mode operation, at steady state with different alkanes acting as induced condensing agents (ICA). The model compares the results for two alkanes: iso-butane and propane. Some results using n-hexane as the ICA agent are also available. The objective of using different ICA's is to study how extensive the co-solubility effects are on reactor's behavior.

This study of the effect of different ICA's on ethylene solubility and polyethylene density shows that n-hexane has the higher influence, leading to higher ethylene solubility and lower density of the polymer amorphous phase. However, this alkane has a low vapor pressure, which greatly limits the amount that can be added to the reactor in dry mode operation. This led to the exclusive use of iso-butane and propane in simulations I through III. The increase in temperature lowers the ethylene solubility in the polymer and lowers polymer density.

The model validation was conducted using the example 7C of US Patent 6864332 B2 [40]. The example was replicated by the developed model, using the same reactor diameter, catalyst bed height, reactor total pressure, ethylene, propane and iso-butane partial pressures. The composition of the feed still was adjusted. The ethylene solubility was predicted combining the values for the solubility for both ICA's. The values predicted by the model deviated from the patent in 4.2% for HDPE Production, 0% for reactor temperature and 0% for superficial gas velocity. As such, the model can be considered reasonably valid.

From simulation I it is possible to conclude that increasing the ICA's partial pressure increases polymer production and lowers the reactor temperature, in general. The observed decrease in mean particle size with increasing ICA is not in agreement with what was expected initially. However, in simulation IV these results were further investigated and it was possible to conclude that for the polymer PSD the temperature is a more important parameter than ethylene solubility. The increase in ICA does not affect other reactor parameters, such as superficial velocity or bed porosity.

Simulation II showed that the range of operating temperature is also an important aspect. The increase in temperature leads to lower a ethylene solubility, but increases the kinetic rate constant. This simulation clearly shows that the catalyst performs better under lower temperature, since effects of the co-solubility are more important than the effects of increasing the temperature.

Simulation III targets a constant production rate and temperature. It is necessary to decrease the inlet flowrate and increase the catalyst feed to keep constant production rate and temperature. This simulation also showed how the superficial velocity influences the reactor behavior. It was proven that a decrease in the superficial velocity leads to a bed contraction.

Simulation IV shows the effect of the different ICA's and solid temperature on the polymer PSD. The bigger the ICA molecule, the bigger the co-solubility effect is and therefore bigger polymer particles are formed. The mean particle size increases with the increase of ICA when the temperature is kept constant. The model is very sensitive to the ICA that is used. The increase in temperature leads to bigger particles.

From the sensitivity analysis, it is possible to conclude that the most important parameter that influences the model outputs is the catalyst's activity. Contrary to what was expected, the alkane's partial pressure does not have much influence on production. The inlet temperature also didn't affect the system as expected, since it affected the pressure drop a lot more significantly than the bulk temperature.

For future work, this model would greatly benefit with:

- A PSD model that accounts for the catalyst sites deactivation;
- A detailed model for the bed fluidization;
- Modeling of condensed mode operation;
- Adaptation of the model to transient state;
- Addition of a polymer PSD inside the reactor, so that more than one mean particle size is considered;
- Incorporation of a reliable thermodynamic model that allows the user to consider more components in the reactor;
- Introduction of a more complex thermodynamic model to predict the properties of the gas phase;

The evaluation of the cost/benefit of further developing this model by introducing more complexity is also an important issue to be taken into account.

References

- [1] A. J. Peacock, *Handbook of Polyethylene: Structures: Properties and Applications*, 1st editio. CRC Press, 2000.
- [2] J. B. P. Soares and T. F. L. McKenna, *Polyolefin Reaction Engineering*. Wiley-VCH, 2012.
- [3] Y. V. Kissin, *Polyethylene: End-Use Properties and their Physical Meaning*, First. New Jersey: Hanser Publishers, 2013.
- [4] D. B. Malpass, *Industrial Polyethylene: Properties, Catalyst, Processes*. Wiley, 2010.
- [5] Y. Kawai, *Global Outlook of Polyolefin Business*. Sumitomo Chemical (Asia Pacific) Pte Ltd, 2013.
- [6] T. C. Mun, "Production of polyethylene Using Gas Fluidized Bed Reactors," 2012.
- [7] J. M. Jenkins, R. L. Jones, T. M. Jones, and S. Beret, "Method for Fluidized Bed Polymerization," Patent 4,588,790, 1986.
- [8] "Innovene G process." [Online]. Available: <http://www.ineos.com/businesses/ineos-technologies/technologies/>. [Accessed: 22-Mar-2016].
- [9] "Spherilene process." [Online]. Available: <https://www.lyondellbasell.com/globalassets/products-technology/technology/spherilene-brochure.pdf>. [Accessed: 22-Mar-2016].
- [10] T. Xie, K. B. McAuley, J. C. C. Hsu, and D. W. Bacon., "Gas phase ethylene polymerization: Production processes, polymer properties, and reactor modeling," *Ind. Eng. Chem. Res.*, vol. 33, no. 3, pp. 449–479, 1994.
- [11] A. Wonders, G. E. Moore, R. R. Ford, F. D. Daily, K. A. Dooley, and J. J. Garcia, "Suppression of Fines in Fluid Bed Polyethylene Process," Patent US 5969061, 1999.
- [12] R. E. Pequeno, R. O. Hagerty, and B. Savatsky, "Bulk Density Promoting Agents in a Gas-phase Polymerization Process to Achieve a Bulk Particle Density," US 7754834 B2, 2010.
- [13] Y. Banat, F. Al-Obaidi, and A. K. MAlek, "Olefin Gas Phase Polymerisation," Patente US 8669334 B2, 2014.
- [14] M. A. Bashir, M. Al-haj Ali, V. Kanellopoulos, and J. Sepp??I??, "Modelling of multicomponent olefins solubility in polyolefins using Sanchez-Lacombe equation of state," *Fluid Phase Equilib.*, vol. 358, pp. 83–90, 2013.
- [15] A. Novak, M. Bobak, J. Kosek, B. J. Banaszak, D. Lo, T. Widya, W. Harmon Ray, and J. J. de Pablo, "Ethylene and 1-hexene sorption in LLDPE under typical gas-phase reactor conditions: Experiments," *J. Appl. Polym. Sci.*, vol. 100, no. 2, pp. 1124–1136, Apr. 2006.
- [16] W. Yao, X. Hu, and Y. Yang, "Modeling solubility of gases in semicrystalline polyethylene," *J. Appl. Polym. Sci.*, vol. 103, no. 3, pp. 1737–1744, Feb. 2007.
- [17] M. A. Bashir, V. Monteil, V. Kanellopoulos, M. A.-H. Ali, and T. McKenna, "Partial Molar Volumes and Thermal Expansion Coefficients as an Explanation for Co-Solvent Effect of Penetrants in Multicomponent Polymer Mixtures," *Macromol. Chem. Phys.*, vol. 216, no. 21, pp. 2129–2140, Nov. 2015.
- [18] D. Kunii and O. Levenspiel, *Fluidization Engineering*, 2nd editio. Reed Publishing Inc., 1991.
- [19] J. Davidson and D. Harrison, *Fluidized particles*. Cambridge University Press, 1963.
- [20] Y. Wen-Ching, *Handbook of Fluidization and Fluid-Particle Systems*. CRC Press, 2003.
- [21] K. Y. Choi and W. H. Ray, "The dynamic behavior of fluidized bed reactors for solid catalysed gas phase olefin polymerization," *Chem. Eng. Sci.*, vol. 40(12), pp. 2261–2279, 1985.
- [22] W. E. Grosso and M. G. Chiovetta, "Modeling a fluidized-bed reactor for the catalytic

- polimerization of ethylene: particle size distribution effects," *Lat. Am. Appl. Res.*, vol. 35, pp. 67–76, 2005.
- [23] H. Hatzantonis, H. Yiannoulakis, A. Yiagopoulos, and C. Kiparissides, "Recent developments in modeling gas-phase catalyzed olefin polymerization fluidized-bed reactors: the effect of bubble size variation on the reactor's performance," *Chem. Eng. Sci.*, no. 55, p. 3237, 2000.
- [24] K. McAuley, J. P. Talbot, and T. Harris, "A Comparison of Two-Phase and Well Mixed Models for Fluidized Bed Polyethylene Reactors," *Chem. Eng. Sci.*, vol. 49(13), pp. 2261–2279, 1994.
- [25] D. M. Cecílio, "Modelling of Gas and Slurry Phase Polyolefin Production : The importance of thermodynamics," 2015.
- [26] J. B. Soares and A. E. Hamielec, "Effect of reactor residence time distribution on the size distribution of polymer particles made with heterogeneous ziegler-natta and supported metallocene catalysts. a generic mathematical model," *Macromol. Theory Simulations*, vol. 4(6), pp. 1085–1104, 1995.
- [27] P. . J. T. Tait, *Comprehensive Polymer Science*. Oxford, 1989.
- [28] L. Noristi, E. Marchetti, G. Baruzzi, and P. Sgarzi, "Investigation on the particle growth mechanism in propylene polymerization with MgCl₂-supported ziegler–natta catalysts," *J. Polym. Sci., Part A Polym. Chemistry*, vol. 32, pp. 3047–3059, 1994.
- [29] C. W. Hock, "How TiCl₃ Catalysts Control the Texture of As-Polymerized Polypropylene," *J. Polym. Sci., Part A Polym. Chemistry*, vol. 3, no. 12, pp. 3055–3064, 1966.
- [30] J. J. Boor, *Ziegler-Natta Catalysts and Polymerization*. New York: Academic Press, 1979.
- [31] M. Kakugo, H. Sadatoshi, J. Sakai, and M. Yokoyama, "Growth of polypropylene particles in heterogeneous Ziegler-Natta polymerization," *Macromolecules*, vol. 22, no. 7, pp. 3172–3177, 1989.
- [32] P. Galli and J. C. Haylock, "Advances in Ziegler-Natta polymerization - unique polyolefin copolymers, alloys and blends made directly in the reactor," *Makromol. Chemie. Macromol. Symp.*, vol. 22, no. 1, pp. 19–54, 1992.
- [33] K. B. McAuley, J. P. Talbot, and T. J. Harris, "A comparison of two-phase and well-mixed models for fluidized-bed polyethylene reactors," *Chem. Eng. Sci.*, vol. 49, no. 13, pp. 2035–2045, 1994.
- [34] J. P. Talbot, "The Dynamic Modeling and Particle Effects on a Fluidized Bed Polyethylene Reactor," Queen's University, 1990.
- [35] S. Floyd, K. Y. Choi, T. W. Taylor, and W. H. Ray, "Polymerization of Olefins through Heterogeneous Catalysis III. Polymer Particle Modelling with an Analysis of Intraparticle Heat and Mass Transfer Effects," *J. Appl. Polym. Sci.*, vol. 32, p. 2935, 1986.
- [36] S. Ergun, "Fluid Flow through Packed Columns," *Chem. Eng. Prog.*, vol. 48, 1952.
- [37] J. M. Coulson and J. F. Richardson, *Chemical Engineering*. Bath Press, 2002.
- [38] R. C. Reid, J. M. Prausnitz, and E. E. Poling, *The Properties of Gases & Liquids*, 4th ed. McGraw Hill.
- [39] Y. S. Wong and P. K. Seville, "Single-particle motion and heat transfer in fluidized beds," *AIChE J.*, vol. 52(12), pp. 4099–4109, 2006.
- [40] A. BRAGANCA, "Process for the gas phase polymerization and copolymerization of olefin monomers," 2005.
- [41] A. Alizadeh, "Study of Sorption, Heat and Mass Transfer During Condensed Mode Operation of Gas Phase Ethylene Polymerization on Supported Catalyst," Queen's University, 2014.
- [42] W. Ray and R. Hutchinson, "Polymerization of olefins through heterogeneous catalysis. VIII. monomer sorption effects.," *J. Appl. Polym. Sci.*, vol. 41, no. 1, pp. 51–81, 1990.
- [43] J. Kosek and Z. G., "Dynamics of particle growth and overheating in gas-phase polymerization reactors.," *Chem. Eng. Sci.*, vol. 56, no. 13, pp. 3951–3977, 2001.

- [44] J. Chmelar, P. Matuska, T. Gregor, M. Bobak, F. Fantinel, and J. Kosek, "Softening of polyethylene powders at reactor conditions," *Chem. Eng. J.*, vol. 228, pp. 907–916, Jul. 2013.
- [45] W. M. R. Parrish, "Solubility of isobutane in two high-density polyethylene polymer fluffs," *J. Appl. Polym. Sci.*, vol. 26, no. 7, pp. 2279–2291, Jul. 1981.

Appendix A

The Sanchez Lacombe EOS

The Figure bellow represents the ethylene/polyethylene systems with and without ICA.

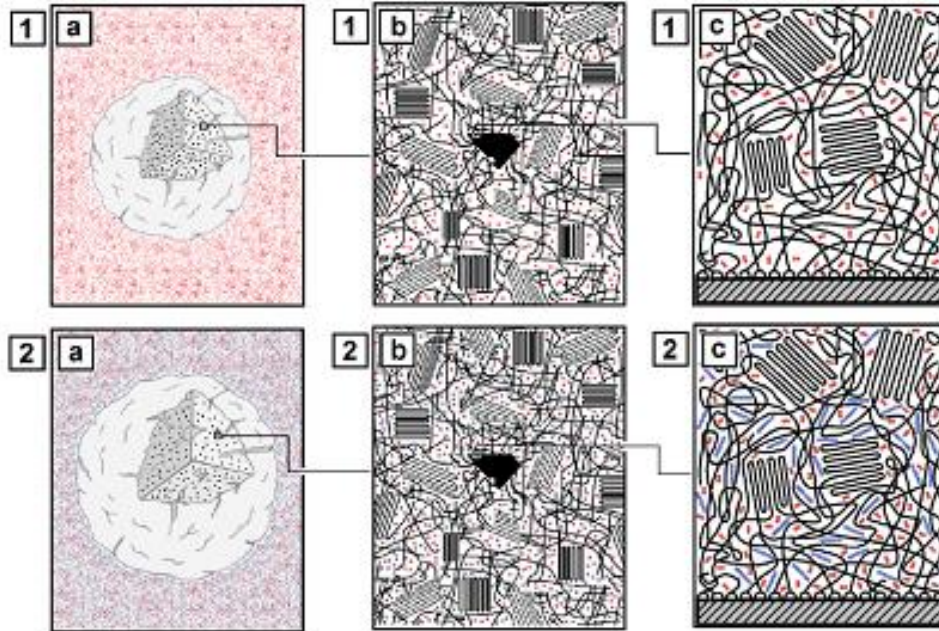


Figure A.1. Schematic representation of: (1) ethylene/polyethylene binary system and (2) ethylene/n-hexane/polyethylene ternary system at different magnifications. Adapted from [41].

The simplified schema in Figure A.1 shows a polymer particle in two distinct systems: a binary one (1) and a ternary one (2). Each schema is divided into three subfigures:

- a: Polymer structure surrounded by a gas phase;
- b: Catalyst fragment (black) surrounded by semi-crystalline polyethylene;
- c: Polymer chains immobilized on the surface of the catalyst fragment

In the first scheme there is only ethylene present with the polymer (in red) and in scheme 2 there is both ethylene (in red) and n-hexane (in blue). The addition of n-hexane causes a phenomenon known as the co-solubility effect. The local ethylene solubility in the polymer phase, increases when n-hexane is added. To adequately model such effect and predict the ethylene solubility, Sanchez-Lacombe thermodynamic model was chosen [41].

The Sanchez-Lacombe Equation of State is written as follows:

$$\bar{\rho}^2 + \bar{P} + \bar{T} \cdot \left[\ln(1 - \bar{\rho}) + \left(1 - \frac{1}{r}\right) \cdot \bar{\rho} \right] = 0 \quad (\text{A.1})$$

Where $\bar{\rho}$, \bar{P} , \bar{T} are the reduced density, pressure and temperature. They are defined as:

$$\bar{T} = T/T^* \quad (\text{A.2})$$

$$\bar{P} = P/P^* \quad (\text{A.3})$$

$$\bar{\rho} = \rho/\rho^* \quad (\text{A.4})$$

where T^* , P^* , ρ^* are, respectively, the characteristic temperature, pressure and close-packed mass density [41].

The model's predictive abilities rely on binary interaction parameters and it has been observed that some parameters are temperature-dependent. Through the study of binary systems such as ethylene/polyethylene and hexane-polyethylene the binary parameters can be adjusted and then employed in a ternary system simulation to predict the necessary concentration [11]. It is important to mention that ethylene is an anti-solvent for the heavier component.

A thermodynamic model that predicts equilibrium monomer concentration at the catalyst sites from bulk gas-phase monomer concentration is present in [42]. In [43] the advantages of steady-state modelling and the possibility of dependence of temperature and concentrations (inside the particles) on model parameters were analyzed.

In systems for which the heat and mass transfer resistances do not influence monomer concentration and temperature within the particles, it was observed that the monomer concentration at the active sites is determined by the equilibrium sorption of the monomer in the polymer particles.

The experimental solubility data of various alkane ICAs in polyethylene at different conditions was taken from the references shown in Table A.0.1. The SL EoS was fitted to these solubility data points in order to obtain the binary interaction parameter for each binary system. These binary interaction parameters were then employed in the SL EoS to estimate the solubility of each gaseous component in the polymer phase and the polymer phase density in the ternary systems i.e., ethylene/ICA/polyethylene.

Table A.0.1. Diluent/PE binary systems considered in this work.

Diluent/PE	Temperature range (°C)	Polymer crystallinity (%wt)	Reference
C ₂ /LLDPE	70 - 150	59 - 61.2	[15]
C ₃ /LLDPE	70	56	[44]
i-C ₄ /HDPE	66 - 94	76	[45]
i-C ₄ /LLDPE	66 - 94	69	[45]
n-C ₆ /LLDPE	70 - 90	72	[16]

Figure A.2. below shows the overall solubility of ethylene/iso-butane mixtures with different gas phase compositions by using the binary interaction parameters obtained by fitting the respective binary experimental solubility data.

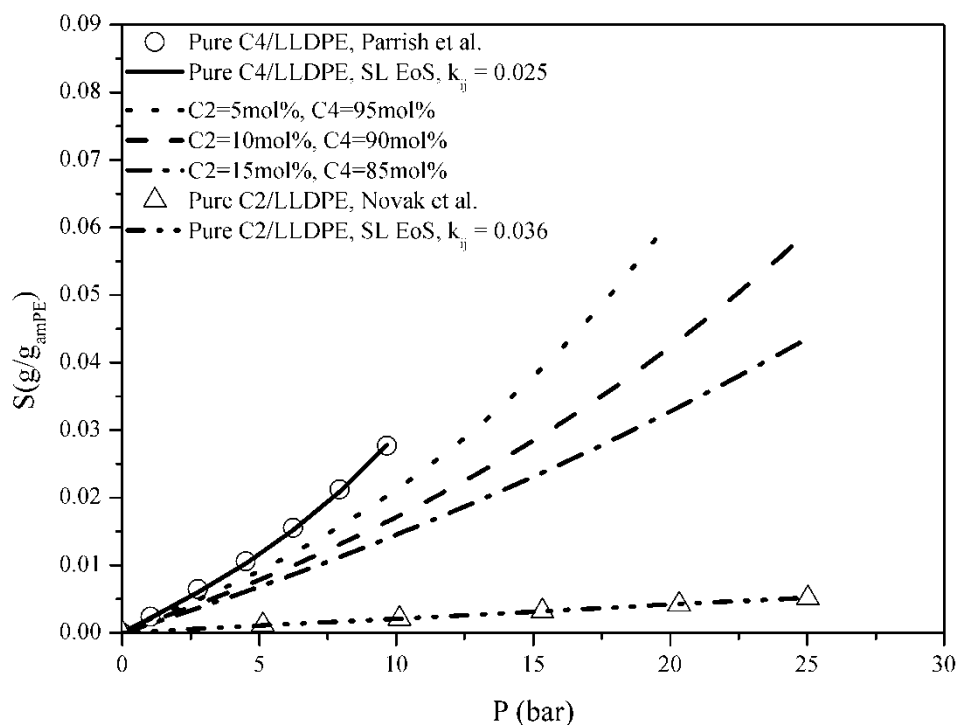


Figure A.2. Solubility of iso-butane, ethylene and their mixtures in LLDPE at 74°C. Fitting of the SL-EoS to binary experimental solubility data of iso-butane(1)/LLDPE(2) and ethylene(1)/LLDPE(2) systems at 74°C is shown for comparison. Experimental solubility data of ethylene(1)/LLDPE(2) obtained from [15].

In addition to excellent fitting results, Figure A.2. shows the overall solubility of ethylene/iso-butane mixtures with different gas phase compositions by using the binary interaction parameters obtained by fitting the respective binary experimental solubility data. As the iso-butane concentration in the gas phase increases, the overall mixture solubility increases and tends to shift towards the pure iso-butane/LLDPE system. The density of the swollen polymer phase decreases with increasing iso-butane content in the gas phase which is in agreement with the fact that the higher the solubility of a penetrant the higher is the swelling of the polymer. The same trends were also observed for all the other systems discussed.

Appendix B

Gas-phase Properties

Heat capacity

The equation that describes the heat capacity of a gaseous component at a given temperature (T) is described by the following equation [38]:

$$C_p = A + B \cdot T + C \cdot T^2 + D \cdot T^3 \quad (\text{B.1})$$

The temperature chosen was that of the reactor as we have assumed that both phases are well mixed.

In the developed model, it is necessary to consider a mean heat capacity, calculated between the inlet flow temperature (T_{in}) and the bulk phase reactor temperature (T_b). This is achieved by integrating equation (B.1) between T_{in} and T_b :

$$\bar{C}_p = \int_{T_{in}}^{T_b} (A + B \cdot T + C \cdot T^2 + D \cdot T^3) dT \quad (\text{B.2})$$

The result is described in the following equation:

$$C_p = \frac{\left[A \cdot (T_b - T_{in}) + \frac{B}{2} \cdot (T_b^2 - T_{in}^2) + \frac{C}{3} \cdot (T_b^3 - T_{in}^3) + \frac{D}{4} \cdot (T_b^4 - T_{in}^4) \right]}{(T_b - T_{in})} \quad (\text{B.3})$$

The parameters A, B, and C were taken from reference [38] with T in K and C_p in J.mol⁻¹.K⁻¹. The values are summarized in Table A.1.

Table B.1 - Component parameters for heat capacity calculations [38].

Component	Ethylene	Propane	n-hexane	Iso-butane	Nitrogen
A	3.806	-4.224	-4.413	-1.39	31.15
B	1.57x10 ⁻¹	3.06x10 ⁻¹	5.82x10 ⁻¹	3.85x10 ⁻¹	-1.36x10 ⁻²
C	-8.35x10 ⁻⁵	-1.59x10 ⁻⁴	-3.12x10 ⁻⁴	-1.85x10 ⁻⁴	2.68x10 ⁻⁵
D	1.76x10 ⁻⁸	3.22x10 ⁻⁸	6.49x10 ⁻⁸	2.90x10 ⁻⁸	-1.17x10 ⁻⁸

Viscosity and Thermal Conductivity

Correlations were developed using data from the *Aspen Plus*TM thermodynamic properties data base to relate the gas-phase viscosity and thermal conductivity with the ICA pressure at 70° and 80°. The generic form of these correlation is:

$$W = A \cdot P_{ICA} + B \quad (\text{B.4})$$

Where W is the desired parameter (viscosity or thermal conductivity of the gas-phase), P_{ICA} is the ICA partial pressure and A and B are the correlation coefficients. For the correlations a fixed total pressure of 20 bar, a fixed ethylene partial pressure of 7 bar and an ICA partial pressure changing between 0 and 11 bar, depending upon the type of ICA, is considered. The nitrogen partial pressure decreases with the increase of the ICA partial pressure in order to keep the total pressure constant.

Table B.2 below shows the coefficients of viscosity, whereas, Table B.2 shows the coefficients of thermal conductivity equation for each ICA and temperature:

Table B.2 Coefficients for the viscosity (Pa.s) correlations.

		Propane	Iso-butane	n-hexane
70°C	A	$-5,517 \times 10^{-7}$	$-4,951 \times 10^{-7}$	-
	B	$1,749 \times 10^{-5}$	$1,798 \times 10^{-5}$	-
80°C	A	-	$-4,950 \times 10^{-7}$	$-8,606 \times 10^{-7}$
	B	-	$1,796 \times 10^{-5}$	$1,433 \times 10^{-5}$

Table B.3. Coefficients for the thermal conductivity ($\text{W} \cdot \text{m}^{-1} \cdot \text{K}^{-1}$) correlations

		Propane	Iso-butane	n-hexane
70°C	A	$-2,856 \times 10^{-4}$	$-3,474 \times 10^{-4}$	-
	B	$2,921 \times 10^{-2}$	$2,921 \times 10^{-2}$	-
80°C	A	-	$-3,474 \times 10^{-4}$	$-1,624 \times 10^{-3}$
	B	-	$2,924 \times 10^{-2}$	$2,855 \times 10^{-2}$

Convective Heat Transfer Coefficient

The convective heat transfer coefficient was estimated using the correlation of Wong and Seville (2006), for Geldart Group B particles [39]:

$$h = 35.8 \cdot K_g^{0.2} \cdot \rho_{PE}^{0.6} \cdot d_p^{-0.36} \quad (\text{B.5})$$

Where h represents the convective heat transfer coefficient ($\text{W}\cdot\text{m}^{-2}\cdot\text{K}^{-1}$), K_g the gas thermal conductivity, ρ_{PE} the polymer density and d_p the polymer particle size.

Gas-phase Density

The gas-phase density is estimated using the ideal gas law, since the mixture is composed of hydrocarbons and an inert gas, molecules that don't stray from the ideal gas behavior.

$$Q_{V,n} = \frac{Q_{m,n} \cdot R \cdot T_b}{MW_n \cdot P} \quad (\text{B.6})$$

Where $Q_{V,n}$ and $Q_{m,n}$ represent the volumetric and mass flowrate for the n component. R is the ideal gas constant and MW_n is the n component molecular weight.

Appendix C

Simulations Data

In this section the data for the simulations I through III and the ICA effect on Ethylene Solubility and polymer density will be presented. Simulation IV and all other polymer PSD values will not be presented due to their excessive size.

ICA effect on Ethylene Solubility and polymer density

The values for the iso-butane solubility in amorphous polymer phase and effect on ethylene solubility and polymer density at 80°C are presented in Table C.1.

Table C.1. Iso-butane solubility (C_{ICA}^P) and effect on ethylene solubility (C_{et}^P) and amorphous polymer density (ρ_{PE}) at 80°C [45].

iso-Butane Partial Pressure (bar)	C_{et}^P (mol/m ³)	C_{ICA}^P (mol/m ³)	ρ_{PE} (kg/m ³)
0	129,5	0,0	825,4
1	134,8	121,6	821,8
3	142,6	342,7	816,2
7	160,6	790,5	804,6
13	192,5	1597,3	782,7

The values for the iso-butane solubility in amorphous polymer phase and effect on ethylene solubility and polymer density at 70°C are presented in Table C.2.

Table C.2. Iso-butane solubility (C_{ICA}^P) and effect on ethylene solubility (C_{et}^P) and amorphous polymer density (ρ_{PE}) at 70°C [45].

iso-Butane Partial Pressure (bar)	C_{et}^P (mol/m ³)	C_{ICA}^P (mol/m ³)	ρ_{PE} (kg/m ³)
0	152,4	0,0	829,0
0,1	153,7	36,1	828,5
0,7	156,0	184,7	826,7
1,2	158,6	290,8	825,5
1,5	159,0	366,6	824,6
3,4	167,5	788,1	819,5
5,1	177,0	1182,0	814,7
7,9	190,8	1891,7	806,0

The values for the propane solubility in amorphous polymer phase and effect on ethylene solubility and polymer density at 70°C are presented in Table C. 3.

Table C. 3. Propane solubility (C_{ICA}^P) and effect on ethylene solubility (C_{et}^P) and amorphous polymer density (ρ_{PE}) at 70°C [44].

Propane Partial Pressure (bar)	C_{et}^P (mol/m³)	C_{ICA}^P (mol/m³)	ρ_{PE} (kg/m³)
0	152,4	0,0	829,0
0,2	153,1	97,4	828,6
1,0	155,6	99,0	827,2
1,6	156,7	99,7	826,2
2,0	156,3	99,5	825,5
4,5	162,2	103,2	821,4
10,4	175,5	111,7	811,1

The values for the n-hexane solubility in amorphous polymer phase and effect on ethylene solubility and polymer density at 80°C are presented in Table C.4.

Table C.4. n-Hexane solubility (C_{ICA}^P) and effect on ethylene solubility (C_{et}^P) and amorphous polymer density (ρ_{PE}) at 80°C

n-Hexane Partial Pressure (bar)	C_{et}^P (mol/m³)	C_{ICA}^P (mol/m³)	ρ_{PE} (kg/m³)
0	129,5	0,0	825,4
0,1	132,2	34,4	824,0
0,5	137,4	171,4	820,4
0,8	139,9	271,4	817,7
1,0	145,4	346,4	815,7

Simulation I – Comparison between the addition of Iso-butane Vs Propane

The values for the simulation results are presented in Tables C.5. and C.6. for propane and Iso-butane, respectively.

Table C.5. Results for propane at 70°C simulation I.

Propane Partial Pressure (bar)									
Parameter	Units	0	1	2	3	4	5	6	7
Temperature bulk	°C	74	73	71	70	69	68	67	66
Temperature solids	°C	87	85	84	82	81	80	79	78
Pressure drop	bar	1,9	1,9	2,0	2,0	2,1	2,2	2,3	2,4
Per pass conversion	%	4,3	4,4	4,5	4,6	4,6	4,7	4,7	4,8
Productivity	g _{polymer} /g _{catlyst}	3868	3948	4017	4082	4141	4190	4234	4269
Production Rate	ton/h	15,3	15,6	15,9	16,2	16,4	16,6	16,8	16,9
Residence time	h	5,08	4,94	4,82	4,72	4,65	4,59	4,55	4,52
Bed Porosity	-	0,602	0,604	0,606	0,607	0,607	0,606	0,605	0,603
Mean Particle size	µm	714	698	683	671	659	649	640	631
Superficial Velocity	m/s	0,815	0,811	0,808	0,805	0,802	0,800	0,797	0,795

Table C.6. Results for iso-butane at 70°C simulation I and II.

Iso-butane Partial Pressure (bar) (70°C)						
Parameter	Units	0	1	2	3	4
Temperature bulk	°C	74	73	71	70	69
Temperature solids	°C	87	85	84	82	81
Pressure drop	bar	1,9	1,9	2,0	2,0	2,1
Per pass conversion	%	4,3	4,4	4,5	4,6	4,6
Productivity	g _{polymer} /g _{catlyst}	3868	3948	4017	4082	4141
Production Rate	ton/h	15,3	15,6	15,9	16,2	16,4
Residence time	h	5,08	4,81	4,58	4,39	4,24
Bed Porosity	-	0,602	0,606	0,609	0,610	0,611
Mean Particle size	µm	714	696	683	671	662
Superficial Velocity	m/s	0,815	0,811	0,807	0,804	0,801

Simulation II – Iso-butane at 70°C Vs 80°C

The results for simulation II are presented in Table C.6. and Table C.7. for iso-butane at 70°C and 80°C, respectively.

Table C.7. Results for iso-butane at 80°C simulation II.

Iso-butane Partial Pressure (bar) (80°C)						
Parameter	Units	0	1	2	3	4
Temperature bulk	°C	83	81	80	78	77
Temperature solids	°C	99,7	98,3	97,0	95,8	94,8
Pressure drop	bar	1,9	1,9	2,0	2,1	2,2
Per pass conversion	%	5,4	5,7	5,9	6,1	6,4
Productivity	g _{polymer} /g _{catalyst}	3323	3482	3632	3769	3904
Production Rate	ton/h	19,1	20,1	20,9	21,7	22,5
Residence time	h	4,01	3,78	3,58	3,43	3,29
Bed Porosity	-	0,606	0,609	0,612	0,613	0,614
Mean Particle size	µm	748	732	720	709	701
Superficial Velocity	m/s	0,836	0,832	0,828	0,824	0,821

Simulation III – Constant production rate and temperature

The results for simulation III are presented in Table C.8 and Table C.9 for propane and iso-butane, respectively.

Table C.8 . Results for simulation III with propane at 74°C and constant production rate of 15,8 ton/h.

Propane Partial Pressure (bar) (T _b =74 °C)								
Parameter	Units	0	1	3	4	5	7	9
Catalyst Inlet flowrate	kg/s (x10 ⁻⁴)	9,5	9,9	10,6	11,0	11,5	11,9	12,0
Gas Inlet flowrate	mol/s	11500	10800	10000	9250	8500	8000	7500
Superficial Velocity	m/s	0,93	0,87	0,80	0,74	0,69	0,65	0,60
Productivity	g _{polymer} /g _{catalyst}	4619	4347	4122	3914	3751	3712	3684
Per pass Conversion	%	3,89	4,06	4,45	4,78	5,17	5,62	6,00
Pressure Drop	bar	1,51	1,67	1,98	2,30	2,71	3,30	4,05
Bed Porosity	-	0,67	0,64	0,61	0,58	0,56	0,54	0,53
Mean Particle size	µm	642	652	663	686	712	721	728

Table C.9. Results for simulation III with iso-butane at 74°C and constant production rate of 15,8 ton/h.

Iso-butane Partial Pressure (bar) ($T_b=74$ °C)						
Parameter	Units	0	1	2	3	4
Catalyst Inlet flowrate	kg/s ($\times 10^{-4}$)	9,5	10	10,5	10,83	11
Gas Inlet flowrate	mol/s	11500	10900	10100	9300	8500
Superficial Velocity	m/s	0,93	0,88	0,81	0,74	0,68
Productivity	$g_{\text{polymer}}/g_{\text{catalyst}}$	4619	4472	4267	4084	4000
Per pass Conversion	%	3,89	4,18	4,52	4,90	5,27
Pressure Drop	bar	1,51	1,67	1,91	2,24	2,59
Bed Porosity	-	0,67	0,64	0,62	0,59	0,57
Mean Particle size	μm	642	652	663	686	712

Appendix D

Model Code

In this appendix the code for the model will be presented. The several auxiliary files will be presented in the same order as they appear in the main file.

Main File – “Simulations”

File used to run the full model by running it in the Matlab command window.

```
clc
clear all
close all
%
%% Reactor Conditions Overview %%
% the partial pressure of iso-butane can vary between 0 and 4 bar (for
Tinlet=35°C);
% the partial pressure of n-hexane can vary between 0 and 0.3 bar (for
Tinlet=35°C);
% the partial pressure of propane can vary between 0 and 11 bar (for
Tinlet=35°C);
% the partial pressure of ethylene is kept constant at 7 bar;
% the total pressure is kept constant with nitrogen;
% the inlet temperature is kept constant.
%
global T0 P_Et P_ICA P F Qc dc Tb Ts l Fdp0_fraction fluid_porosity dp
Ts_cat_PSD Residence_Time_PSD Popular_size dc_sim
%
%
% Catalyst PSD
%The catalyst diameter (dc_sim) needs to be between 0.049 and 0.0081 cm
dc_sim=[0.0049 0.0055 0.0063]; % Catalyst Diameter (cm)
%
%
Fdp0=zeros(1,length(dc_sim));
Fdp0_total=0;
Fdp0_fraction=zeros(1,length(dc_sim));
for l=1:length(dc_sim)
    Fdp0(l)=-16082.33741*dc_sim(l)^2+203.7601047*dc_sim(l)-0.424219368;
    Fdp0_total=Fdp0_total+Fdp0(l);
end
%
for l=1:length(dc_sim)
    Fdp0_fraction(l)=(Fdp0(l)/Fdp0_total);
end
%
%%%%%%%%%%%%%%%%%%%%%%%%%%%%%%%%%%%%%%%%%%%%%%%%%%%%%%%%%%%%%%%%%%%%%%%%
%
%% Simulation Iso-butane P_total=20 bar and Thermodynamic data at 70°C %%
% Inlet flowrates, Temperature and Pressure
%
F = 10000; % Total Inlet Flowrate (mol/s)
Qc = 0.0011; % Catalyst Mass Flow (kg.s-1)
T0=35+273.15; % inlet temperature (K)
P_Et = 7; % Ethylene Partial Pressure in
Reactor (Bar)
P_ICA_sim = [0 1 2 3 4]; % ICA Partial Pressure in
Reactor (Bar)
P=20; % Total Pressure (bar)
%
%% Guess Matrix (inicial values for solver) %
```

```

% guess=[Q_Et_out Q_Et_d Q_ICA_out Q_ICA_d kp Rp Q_PE kd
Cstar Cpg_Et Cpg_ICA Cpg_N2 Tb Ts Q_Et_in Q_ICA_in Q_N2_in
Qv_Total_in Superficial Velocity rho_gas etha arq u_mf Ratio u_t
slop OO fluid_porosity_iteration Vp np Vc Apc rho_b]
%
%Guess 1 - For P_ICA=0 bar

%%
Variables_Inicialization; % Initializes the variables
which will store the simulation values
deviation_dp=1; % Auxiliary variable to aid in
converging the mean particle size iteration
deviation_porosity=1; % Auxiliary variable to aid in
converging the bed porosity iteration
%
for r=1:1:length(P_ICA_sim)
    dp = 650e-06;
    fluid_porosity=0.58;
    P_ICA=P_ICA_sim(r);
    deviation_porosity=1;
    while deviation_porosity>0.0001
        for l=1:length(dc_sim)
            while deviation_dp>2*10^-6
                dc=dc_sim(l)
                if P_ICA==0
                    guess=guess_sim1(l,:);
                else
                    guess=guess_sim2(l,:);
                end
                solver_isobutane;
                Residence_Time_PSD=Residence_Time;
                Ts_cat_PSD=Ts;
                PSD; % Initializes the file that contains the PSD model
                PSD_Dp_Save(:,l)=Dp;
                PSD_F_Dp_Save(:,l)=F_Dp;
                deviation_dp=abs(dp-Popular_size);
                dp=Popular_size;
            end
            deviation_dp=1;
            Save_Variables1 % Initializes the file that
saves the average reactor properties
        end
        Save_Variables2 % Initializes the file that
resets auxiliary variables to compute average reactor properties
        deviation_porosity=abs(fluid_porosity-Porosity_save(r));
        fluid_porosity=Porosity_save(r);
    end
    PSD_SUM % Initializes the file that sums
the PSD's for different catalyst sizes
    if r==1
        graph_x_save1=graph_x;
        graph_y_save1=graph_y;
    elseif r==2
        graph_x_save2=graph_x;
        graph_y_save2=graph_y;
    elseif r==3
        graph_x_save3=graph_x;
        graph_y_save3=graph_y;
    elseif r==4
        graph_x_save4=graph_x;
        graph_y_save4=graph_y;
    elseif r==5
        graph_x_save5=graph_x;
        graph_y_save5=graph_y;
    end
end
%
disp('The model has converged')

```

```

%
figure(1), hold on
plot(graph_x_save1,graph_y_save1,'m'), hold on
plot(graph_x_save2,graph_y_save2,'c'), hold on
plot(graph_x_save3,graph_y_save3,'g'), hold on
plot(graph_x_save4,graph_y_save4,'y'), hold on
plot(graph_x_save5,graph_y_save5,'c'), hold on
title('PSD','FontSize',20)
xlabel('D_P (microns)','FontSize',16)
ylabel('Volume Density (%)','FontSize',16)
axis([0 1700 0 11])
set(gca,'FontSize',14);
h_legend=legend('P_I_S_O_B_U_T=0 Bar','P_I_S_O_B_U_T=1 Bar','P_I_S_O_B_U_T=2
Bar','P_I_S_O_B_U_T=3 Bar','P_I_S_O_B_U_T=4 Bar');
set(h_legend,'FontSize',16);
hold off
%%%%%%%%%%%%%%%%%%%%%%%%%%%%%%%%%%%%%%%%%%%%%%%%%%%%%%%%%%%%%%%%%%%%%%%%
figure(2), hold on
subplot(1,2,1),plot(P_ICA_sim,Tb_save,'.-m'), hold on
title('Average Bulk Temperature','FontSize',24)
xlabel('P_I_s_o_b_u_t_a_n_e (bar)','FontSize',18)
ylabel('Temperature (°C)','FontSize',18)
set(gca,'FontSize',16);
subplot(1,2,2),plot(P_ICA_sim,P_drop_save,'.-m'), hold on
title('Reactor Pressure Drop','FontSize',24)
xlabel('P_I_s_o_b_u_t_a_n_e (bar)','FontSize',18)
ylabel('DeltaP (bar)','FontSize',18)
set(gca,'FontSize',16);
hold off
%%%%%%%%%%%%%%%%%%%%%%%%%%%%%%%%%%%%%%%%%%%%%%%%%%%%%%%%%%%%%%%%%%%%%%%%
figure(3)
subplot(1,2,1),plot(P_ICA_sim,Porosity_save,'.-m'), hold on
title('Bed Porosity','FontSize',24)
xlabel('P_I_s_o_b_u_t_a_n_e (bar)','FontSize',18)
ylabel('Bed Porosity (-)','FontSize',18)
set(gca,'FontSize',16);
subplot(1,2,2),plot(P_ICA_sim,Superficial_Velocity_save,'.-m'), hold on
subplot(1,2,2),plot(P_ICA_sim,u_t_save,'.-c'), hold on
subplot(1,2,2),plot(P_ICA_sim,u_mf_save,'.-b'), hold on
title('Superficial Velocity','FontSize',24)
xlabel('P_I_s_o_b_u_t_a_n_e (bar)','FontSize',18)
ylabel('Superficial Velocity (m/s)','FontSize',18)
h_legend=legend('Superficial velocity','Terminal Velocity','Minimum
fluidisation velocity');
set(h_legend,'FontSize',18);
set(gca,'FontSize',16);
hold off
%%%%%%%%%%%%%%%%%%%%%%%%%%%%%%%%%%%%%%%%%%%%%%%%%%%%%%%%%%%%%%%%%%%%%%%%
figure(4)
subplot(1,2,1),plot(P_ICA_sim,PE_Hourly_save,'.-m'), hold on
title('PE Hourly production','FontSize',24)
xlabel('P_I_s_o_b_u_t_a_n_e (bar)','FontSize',18)
ylabel('PE flowrate (ton/h)','FontSize',18)
set(gca,'FontSize',16);
subplot(1,2,2),plot(P_ICA_sim,Productivity_save,'.-m'), hold on
title('Productivity','FontSize',24)
xlabel('P_I_s_o_b_u_t_a_n_e (bar)','FontSize',18)
ylabel('Productivity (kg_P_E/kg_C_a_t)','FontSize',18)
set(gca,'FontSize',16);
%%%%%%%%%%%%%%%%%%%%%%%%%%%%%%%%%%%%%%%%%%%%%%%%%%%%%%%%%%%%%%%%%%%%%%%%
figure(5)
plot(P_ICA_sim,Per_Pass_Conversion_save,'.-m')
title('Per Pass Conversion','FontSize',24)
xlabel('P_I_s_o_b_u_t_a_n_e (bar)','FontSize',18)
ylabel('Per Pass Conversion (%)','FontSize',18)
set(gca,'FontSize',16);
%

```

Auxiliary file – “Variables_initialization”

File where all the variables used to save simulation values are initialized.

```
%%%%%%%%%%%%%%%%%%%%%%%%%%%%%%%%%%%%%%%%%%%%%%%%%%%%%%%%%%%%%%%%%%%%%%%% Variables Inicialization %%%%%%%%%%
%%
Tb_cat_save=zeros(1,length(dc_sim));
Ts_cat_save=zeros(1,length(dc_sim));
Tb_cat=0;
Tb_save=zeros(1,length(P_ICA_sim));
Ts_save=zeros(1,length(P_ICA_sim));
Ts_cat=0;
Residence_Time_average=0;
Residence_Time_save=zeros(1,length(P_ICA_sim));
Superficial_Velocity_average=0;
Superficial_Velocity_save=zeros(1,length(P_ICA_sim));
P_drop_average=0;
P_drop_save=zeros(1,length(P_ICA_sim));
u_t_average=0;
u_t_save=zeros(1,length(P_ICA_sim));
u_mf_average=0;
u_mf_save=zeros(1,length(P_ICA_sim));
PE_Hourly_average=0;
PE_Hourly_save=zeros(1,length(P_ICA_sim));
Productivity_average=0;
Productivity_save=zeros(1,length(P_ICA_sim));
Porosity_average=0;
Porosity_save=zeros(1,length(P_ICA_sim));
PSD_Dp_Save=zeros(30000,length(dc_sim));
PSD_F_Dp_Save=zeros(30000,length(dc_sim));
dp_average=0;
dp_save=zeros(1,length(P_ICA_sim));
Per_Pass_Conversion_average=0;
Per_Pass_Conversion_save=zeros(1,length(P_ICA_sim));
Rp_average=0;
Rp_save=zeros(1,length(P_ICA_sim));
```

Auxiliary file – “Solver_isobutane”

This file contains the information regarding the system and is where the function *solver* is implemented. It varies for each ICA used and for different temperatures.

```
%%%%%%%%%%%%%%%%%%%%%%%%%%%%%%%%%%%%%%%%%%%%%%%%%%%%%%%%%%%%%%%%%%%%%%%% SYSTEM DESCRIPTION %%%%%%%%%%
%
% Q - Mass Flowrate
% MW - Molecular Weight
% rho - Specific Weight (kg.m-3)
% kp - Kinetic Propagation Constant
% Ea - Activation Energy
% kd - Kinetic Deactivation Constant
% Ed - Deactivation Energy
% C0star - Initial active sites concentration
% Cstar - Active sites concentrations
% omega - Pitzer acentric factor
% ReactHeat - Heat of Reaction
%
%%%%%%%%%%%%%%%%%%%%%%%%%%%%%%%%%%%%%%%%%%%%%%%%%%%%%%%%%%%%%%%%%%%%%%%%
%
global R P Ts T0 Tref Tb F A_Et B_Et C_Et D_Et Cpg_Et A_ICA B_ICA C_ICA D_ICA
A_N2 B_N2 C_N2 D_N2 Cpg_ICA Cpg_N2 Cp_c P_Et P_ICA P_N2 Q_Et_in Q_Et_d
Q_Et_out m_Et m_ICA Q_ICA_in Q_ICA_d Q_ICA_out Q_N2_in Q_PE Qc rho_b Vc Apc Vb
h kp_Tref kd_Tref kp kd Rp C0star Cstar C_Et_P C_ICA_P ReactHeat Ea Ed MW_Et
MW_ICA MW_N2 MW_PE rho_PE Cp_PE Vp np rho_c fluid_porosity dp dc Qv_Total_in
```

```

Superficial_Velocity rho_gas areatrans Re_p etha porosity_mf Arq Re_mf u_mf
P_drop wCD CD u_t OO viscosity hb slop fluid_porosity_iteration Ratio
%
%% Variable Initialization %
%
R = 8.3145; % Perfect Gas Constant in (J/mol.K)
MW_Et = 28.054/1000; % Ethylene Molecular Weight (kg.mol-1)
MW_ICA = 58.12/1000; % ICA Molecular Weight (kg.mol-1)
MW_PE = 2; % PE Molecular Weight (kg.mol-1)
MW_N2 = 28.014/1000; % N2 Molecular Weight (kg.mol-1)
%
%% Gaseous Component Heat Capacity %%
%% Empirical Parameters %%
% Ethylene %
A_Et = 3.806;
B_Et = 1.566e-01;
C_Et = 8.348e-05;
D_Et = 1.755e-08;
%
% ICA - isobutane %
A_ICA = -1.39;
B_ICA = 3.847e-01;
C_ICA = -1.846e-04;
D_ICA = 2.895e-08;
%
% Nitrogen
A_N2 = 3.115e1;
B_N2 = -1.357e-2;
C_N2 = 2.680e-5;
D_N2 = -1.168e-8;

%% %%%%%%%%%%%%%%%%%%%%%%%%%%%%%%%%%%%%%%%%%%%%%%%%%%%%%%%%%%%%%%%%%%%%%%%%%OPERATING CONDITIONS %%%%%%%%%%%%%%%%%%%%%%%%%%%%%%%%%%%%%%%%%%%%%%%%%%%%%%%%%%%%%%%%%%%%%%%%%
% Reactor Parameters %
%
P_N2=P-P_Et-P_ICA; % N2 Partial Pressure in Reactor (bar)
rho_PE = 828.970970005343-2.87602844308952*P_ICA; % PE density (kg/m3)
kp_Tref = 180; % kinetic constant at reference temperature T0 (m3.mol-1.s-1)
kd_Tref = 1e-04; % kinetic deactivation constant at ref. temperature T0 (s-1)
Tref = 353.15;% Reference temp. for propagation and deactivation constants (K)
viscosity=-4.95057463349998*10^(-7)*P_ICA+0.0000174892917010155; % Average
Viscosity (Pa.s) [Aspen Correlation - At 80°C Total pressure of 20 bar. Ranges
Between 0 and 8 bar]
%
% Catalyst Parameters %
%
Cp_c = 2000; % Catalyst Heat Capacity (J.kg-1.K-1)
Cp_PE = 2000; % Polymer Particle Heat Capacity (J.kg-1.K-1)
rho_c = 2300; % Catalyst Specific Weight (kg.m-3)
C0star = 0.52; % Catalyst Initial Active Sites Concentration (mol.m-3)
d = 4.75; % Reactor Diameter (m)
areatrans = pi*0.25*d^2; % Reactor cross-section area (m2)
hb = 13.3; % Reactor height (m)
Vb = hb*areatrans; % Bed Volume (m3)
K_g=-0.000347490096836983*P_ICA+0.0292192212118008; % Gas Thermal Conductivity
(W/m.K) [Aspen Correlation - At 70°C Total pressure of 20 bar. Ranges Between
0 and 8 bar]
h=35.8*(K_g^0.2)*(rho_PE^0.6)*(dp^-0.36); % Convective
Heat Transfer Coefficient (W/m2.K)
%
% Reaction Parameters %
%
Ea = 42000; % Activation Energy (J/mol)
Ed = 42000; % Catalyst Deactivation Energy (J/mol)
ReactHeat = -107600; % Heat of Reaction (J/mol)
C_Et_P = 4.82404386619489*P_ICA + 152.35020129046; % Ethylene Concentration
in growing polymer phase (mol.m-3)
C_ICA_P = 237.691868034532*(P_ICA); % ICA Concentration in
growing polymer phase (mol.m-3)

```

```

%%
%%
%%
%% Bed Properties
rho_b = rho_c*(1-fluid_porosity); % Fluidizes bed density (kg/m3)
Vp = Vb*(1-fluid_porosity); % Particle Volume in catalyst bed (m3)
np = 6/pi*Vp*dp^(-3); % Number of particles in catalyst bed
Vc = np*pi/6*(dc/100)^3; % Catalyst Volume (m3)
Apc = np*pi*(dp/100)^2; % Catalyst Heat Transfer Area (m2)
porosity_mf = 0.476; % Minimum fluidization porosity;

%% Solver
[result, fval, exit, output]=fsolve(@variables,guess);
result;
fval;
output;

%%Pressure drop given by Ergun equation (bar)
P_drop = (150*((1-
porosity_mf)^2/(porosity_mf^3))*(viscosity*u_mf/(dp^2))+1.75*((1-
porosity_mf)/(porosity_mf^3))*((rho_gas*u_mf^2)/dp))*10^-5*hb ;
%
Tsolids=Ts-273.15; % Solids Temperature (°C)
Tbulk=Tb-273.15; % Bulk Temperature (°C)
PE_Hourly=Q_PE*3600/1000; % PE hourly production (ton/h)
Productivity=Q_PE/Qc; % Catalyst Productivity (gpolymer/gcatalyst)
Residence_Time=Vb/(Q_PE_Hourly/(rho_PE*(1-fluid_porosity))); % Reactors
Residence time
Per_Pass_Conversion=Q_PE/Q_Et_in*100; % Per Pas conversion (%)

```

Auxiliary file – “Variables”

The following code contains the variables that are to be calculated by *solvr*.

```

%% REACTION SYSTEM %%
%
function eqs = variables(v)
%
global R Ts T0 P Tref Tb F P Et P_ICA P_N2 A_Et B_Et C_Et D_Et Cpg_Et Cpg_N2
A_ICA B_ICA C_ICA D_ICA A_N2 B_N2 C_N2 D_N2 Cpg_ICA Cp_c Q_Et_in Q_Et_d
Q_Et_out Q_N2_in Q_ICA_in Q_ICA_d Q_ICA_out Q_PE Qc Apc Vb h rho_b Vc kp Tref
kd Tref kp kd Rp C0star Cstar C_Et_P C_ICA_P ReactHeat Ea Ed MW_Et MW_ICA
MW_PE MW_N2 rho_PE Cp_PE Vp np rho_c fluid_porosity dp dc Qv_Total_in
Superficial_Velocity rho_gas areatrans etha porosity_mf Arq Re_mf u_mf P_drop
wCD CD u_t slop OO viscosity hb Ratio fluid_porosity_iteration
%
%% OUTPUT VARIABLES %%%%%%%%%%%%%%%%%%%%%%%%%%%%%%%%%%%%%%%%%%
%
Q_Et_out = v(1); % Ethylene Exit Flowrate (kg/s)
Q_Et_d = v(2); % Dissolved Ethylene Flowrate (kg/s)
Q_ICA_out = v(3); % ICA Exit Flowrate (kg/s)
Q_ICA_d = v(4); % Dissolved ICA Flowrate (kg/s)
kp = v(5); % Kinetic Propagation Constant (m3.mol-1s-1)
Rp = v(6); % Reaction Rate (mol.m-3cat.s-1)
Q_PE = v(7); % Polyethylene Production Flowrate (kg/s)
kd = v(8); % Catalyst Kinetic Deactivation Constant (s-1)
Cstar = v(9); % Catalyst Active Site Concentration (mol/m3)
Cpg_Et = v(10); % Gaseous Ethylene Heat Capacity (J.kg-1.K-1)
Cpg_ICA = v(11); % Gaseous ICAane Heat Capacity (J.kg-1.K-1)
Cpg_N2 = v(12); % Gaseous N2 Heat Capacity (J.kg-1.K-1)
Tb = v(13); % Bulk Temperature (K)
Ts = v(14); % Reaction and Outlet Temperature (K)
Q_Et_in = v(15); % Ethylene Inletflowrate (kg/s)

```



```

Q_ICA_in = v(16); % ICA Inletflowrate (kg/s)
Q_N2_in = v(17); % N2 Inletflowrate (kg/s)
Qv_Total_in = v(18); % Volumetric Inlet Flow (m3/s)
Superficial_Velocity = v(19); % Superficial Velocity (m/s)
rho_gas = v(20); % Gas phase density (kg/m3)
etha = v(21); % etha factor
Arq = v(22); % Archimedes number
u_mf = v(23); % Minimum fluidization velocity (m/s)
Ratio = v(24); % u_mf/u_t
u_t = v(25); % Terminal Velocity
slop = v(26); % Slop for the bed porosity Correlation
OO = v(27); % Intercept for the bed porosity correlation
fluid_porosity_iteration = v(28); % Bed fluidization at operating conditions

%
%% %%%%%%%%%%%%%%%%%%%%%%%%%%%%%%%%%%%%%%%%%%%%%%%%%%%%%%%%%%%%%%%%%%%%%%%%% MASS BALANCES %%%%%%%%%%%%%%%%%%%%%%%%%%%%%%%%%%%%%%%%%%%%%%%%%%%%%%%%%%%%%%%%%%%%%%%%%
%Ethylene Mass Balance (kg/s) %
eqs(1) = (Q_Et_in - Q_Et_d - Rp*Vc*MW_Et) - Q_Et_out;
%Dissolved Ethylene Mass Balance (kg/s) %
eqs(2) = MW_Et*C_Et_P*Q_PE/rho_PE - Q_Et_d;
%ICA Mass Balance%
eqs(3) = Q_ICA_in - Q_ICA_d - Q_ICA_out;
%Dissolved ICA Mass Balance (kg/s) %
eqs(4) = MW_ICA*C_ICA_P*Q_PE/rho_PE - Q_ICA_d;
%Arrhenius Law for kinetic constant (m3/mol.s) %
eqs(5) = kp_Tref*exp(Ea/R*(1/Tref-1/Ts))- kp;
%Kinetic Rate Law (mol/m3cat.s) %
eqs(6) = kp*Cstar*C_Et_P- Rp;
%Polyethylene Production Mass Balance (kg/s)%
eqs(7) = Rp*Vc*MW_PE/(MW_PE/MW_Et)- Q_PE;
%Arrhenius Law for deactivation constant (s-1) %
eqs(8) = kd_Tref*exp(Ed/R*(1/Tref-1/Ts))- kd;
%Active sites concentration Balance (mol/m3cat) %
eqs(9) = C0star/(1+kd*Vc/(Qc/rho_b))- Cstar;
%% %%%%%%%%%%%%%%%%%%%%%%%%%%%%%%%%%%%%%%%%%%%%%%%%%%%%%%%%%%%%%%%%%%%%%%%%% Gaseous Component Heat Capacity (J/kg.K) %%%%%%%%%%%%%%%%%%%%%%%%%%%%%%%%%%%%%%%%%%%%%%%%%%%%%%%%%%%%%%%%%%%%%%%%%
%Ethylene
eqs(10) = ((A_Et*(Tb-T0)+B_Et/2*(Tb^2-T0^2)+C_Et/3*(Tb^3-T0^3)+D_Et/4*(Tb^4-
T0^4))/(Tb-T0))/MW_Et- Cpg_Et;
%hexane/ ICA
eqs(11) = ((A_ICA*(Tb-T0)+B_ICA/2*(Tb^2-T0^2)+C_ICA/3*(Tb^3-
T0^3)+D_ICA/4*(Tb^4-T0^4))/(Tb-T0))/MW_ICA- Cpg_ICA;
%Nitrogen
eqs(12) = ((A_N2*(Tb-T0)+B_N2/2*(Tb^2-T0^2)+C_N2/3*(Tb^3-T0^3)+D_N2/4*(Tb^4-
T0^4))/(Tb-T0))/MW_N2- Cpg_N2;
%
%% %%%%%%%%%%%%%%%%%%%%%%%%%%%%%%%%%%%%%%%%%%%%%%%%%%%%%%%%%%%%%%%%%%%%%%%%% HEAT BALANCE (T in K) %%%%%%%%%%%%%%%%%%%%%%%%%%%%%%%%%%%%%%%%%%%%%%%%%%%%%%%%%%%%%%%%%%%%%%%%%
eqs(13) = (ReactHeat*(Q_PE/MW_Et))/(Apc*h)+Ts- Tb;
eqs(14) =
(T0*(Q_N2_in*Cpg_N2+Q_Et_out*Cpg_Et+Q_ICA_out*Cpg_ICA+Q_PE*Cp_PE+Qc*Cp_c)/(Q_P
E*Cp_PE+Qc*Cp_c))-
(Tb*(Q_N2_in*Cpg_N2+Q_Et_out*Cpg_Et+Q_ICA_out*Cpg_ICA)/(Q_PE*Cp_PE+Qc*Cp_c))-
(ReactHeat*(Q_PE/MW_Et)/(Q_PE*Cp_PE+Qc*Cp_c))- Ts;
%
%% %%%%%%%%%%%%%%%%%%%%%%%%%%%%%%%%%%%%%%%%%%%%%%%%%%%%%%%%%%%%%%%%%%%%%%%%% Inlet Mass Flowrates (kg/s) %%%%%%%%%%%%%%%%%%%%%%%%%%%%%%%%%%%%%%%%%%%%%%%%%%%%%%%%%%%%%%%%%%%%%%%%%
eqs(15) = F*P_Et/P*MW_Et- Q_Et_in;
eqs(16) = F*P_ICA/P*MW_ICA- Q_ICA_in;
eqs(17) = F*P_N2/P*MW_N2- Q_N2_in;
eqs(18) = ((Q_Et_in/MW_Et)+(Q_ICA_in/MW_ICA)+(Q_N2_in/MW_N2))*R*Tb/(P*100000)-
Qv_Total_in;
%%%%%%%%%%%%%%%%%%%%%%%%%%%%%%%%%%%%%%%%%%%%%%%%%%%%%%%%%%%%%%%%%%%%%%%% Superficial, terminal and m.f. velocities and bed
porosity %%%%%%%%%%%%%%%%%%%%%%%%%%%%%%%%%%%%%%%%%%%%%%%%%%%%%%%%%%%%%%%%%%%%%%%%%
eqs(19) = Qv_Total_in/areatrans-Superficial_Velocity;
eqs(20) = (Q_Et_in+Q_ICA_in+Q_N2_in)/Qv_Total_in-rho_gas;
eqs(21) = 9.81*(rho_PE-rho_gas)-etha;
eqs(22) = (dp^3)*etha*rho_gas/(viscosity^2)-Arq;
eqs(23) = 0.00114*etha*(dp^2)/viscosity-u_mf;
eqs(24) = 26.6-2.3*log10(Arq)-Ratio;
eqs(25) = u_mf*Ratio-u_t;

```

```

eqs(26) = ((1-porosity_mf)/(u_t-u_mf))-slop;
eqs(27) = 1-slop*u_t-00;
eqs(28) = slop*Superficial_Velocity+00-fluid_porosity_iteration;
%
end

```

Auxiliary file – “PSD”

The PSD file contains the PSD model for each catalyst size.

```

% Based on the model of João B.P. Soares - Effect of reactor residence time
% distribution on the size distribution of polymer particles made with
% heterogenous Ziegler-Natta and supported metallocene catalyst
%
global C0star rho_PE C_Et_P dc Ts_cat_PSD Residence_Time_PSD Popular_size
%
% Global Variables meaning:
%
% kp - Kinetic Propagation Constant (m3.mol-1s-1)
% Residence_Time - Residence time (h)
% t- Polymerization Time (min)
% C_Et_P - Ethylene concentration in the growing polymer phase (mol/m3)
%
Kprop_0=1.87*10^10*(10^3*60); % Propagation constant (cm3/mol.min)
Ea_cal=10000; % Activation energy (cal/mol)
R_cal= 1.99; % Perfect gases constante (cal/mol.K)
m=28; % number-average monomer molecular weight (g/mol)
dc; % Diameter class of catalyst particle (cm) (between 0.003 and 0.0135)
%% PSD expressions for a single reactor %%
%
%Dp - Matrix of particle sizes (cm)
%F_Dp - Matrix of number of particles with each Dp (% volume)
Vtotal=0;
Dp=zeros(1,30000);
F_Dp_vol=zeros(1,30000);
for t=1:1:30000
    kprop=Kprop_0*exp(-Ea_cal/(R_cal*Ts_cat_PSD));
    alpha=(kprop)*(C_Et_P/1000000)*(C0star/1000000)*m/(rho_PE/1000); % (min-1)
    | Combined parameter containing the kinetic information of the reaction as
    | well as other thermodynamically relevant parameters
    Dp(t)=dc*(1+alpha*t)^(1/3) ;
    F_Dp_vol(t)=3*(1+alpha*t)^(2/3)/(alpha*dc)*exp(-
t/(Residence_Time_PSD*60))/(Residence_Time_PSD*60)*((1/6)*pi*(Dp(t))^3);
%volume of particles
    Vtotal=Vtotal+F_Dp_vol(t); %total Volume of particles for each catalyst
end
F_Dp=zeros(1,30000);
for t=1:1:30000
    F_Dp(t)=(F_Dp_vol(t)/Vtotal)*100;
end

%% Most common Particle size for each catalyst size %
Max_number=max(F_Dp);
for t=1:1:30000
    if F_Dp(t)==Max_number
        Popular_size=Dp(t)/100;
    end
end
end

```

Auxiliary file – “Save_variables1”

This file averages the values of the different catalyst sizes simulations.

```

%%%%%%%%%%%%%%%%%%%%%%%%%%%%%%%%%%%%%%%%%%%%%%%%%%%%%%%%%%%%%%%%%%%%%%%% Save Variables 1 %%%%%%%%%%%%%%%%%%%%%%%%%%%%%%%%%%%%%%%%%%%%%%%%%%%%%%%%%%%%%%%%%%%%%%%%%
%
Tb_cat_save(1)=Tb-273.15;
Ts_cat_save(1)=Ts-273.15;
Tb_cat=Tb_cat+(Tb-273.15)*Fdp0_fraction(1);
Ts_cat=Ts_cat+(Ts-273.15)*Fdp0_fraction(1);
Residence_Time_average=Residence_Time_average+Residence_Time*Fdp0_fraction(1);
Superficial_Velocity_average=Superficial_Velocity_average+Superficial_Velocity
*Fdp0_fraction(1);
P_drop_average=P_drop_average+P_drop*Fdp0_fraction(1);
u_t_average=u_t_average+u_t*Fdp0_fraction(1);
u_mf_average=u_mf_average+u_mf*Fdp0_fraction(1);
PE_Hourly_average=PE_Hourly_average+PE_Hourly*Fdp0_fraction(1);
Productivity_average=Productivity_average+Productivity*Fdp0_fraction(1);
Porosity_average=Porosity_average+fluid_porosity_iteration*Fdp0_fraction(1);
Per_Pass_Conversion_average=Per_Pass_Conversion_average+Per_Pass_Conversion*Fd
p0_fraction(1);
Rp_average=Rp_average+Rp*Fdp0_fraction(1);

```

Auxiliary file – “Save_variables2”

This file saves the values of the simulation in the variables initialized in the “Variables_initialization” file and resets auxiliary variables used in the averaging calculations.

```

%%%%%%%%%%%%%%%%%%%%%%%%%%%%%%%%%%%%%%%%%%%%%%%%%%%%%%%%%%%%%%%%%%%%%%%% Save Variables 2 %%%%%%%%%%%%%%%%%%%%%%%%%%%%%%%%%%%%%%%%%%%%%%%%%%%%%%%%%%%%%%%%%%%%%%%%%
%
Tb_save(r)=Tb_cat;
Tb_cat=0;
Ts_save(r)=Ts_cat;
Ts_cat=0;
Superficial_Velocity_save(r)=Superficial_Velocity_average;
Superficial_Velocity_average=0;
P_drop_save(r)=P_drop_average;
P_drop_average=0;
u_t_save(r)=u_t_average;
u_t_average=0;
u_mf_save(r)=u_mf_average;
u_mf_average=0;
PE_Hourly_save(r)=PE_Hourly_average;
PE_Hourly_average=0;
Productivity_save(r)=Productivity_average;
Productivity_average=0;
Residence_Time_save(r)=Residence_Time_average;
Residence_Time_average=0;
Porosity_save(r)=Porosity_average;
Porosity_average=0;
dp_save(r)=dp;
Per_Pass_Conversion_save(r)=Per_Pass_Conversion_average;
Per_Pass_Conversion_average=0;
Rp_save(r)=Rp_average;
Rp_average=0;

```

Auxiliary file – “PSD_SUM”

This file sums the PDS for different catalyst sizes.

```

%%%%%%%%%%%%%%%%%%%%%%%%%%%%%%%%%%%%%%%%%%%%%%%%%%%%%%%%%%%%%%%%%%%%%%%% Summing the PSD for different Dp0 %%%%%%%%%%%%%%%%%%%%%%%%%%%%%%%%%%%%%%%%%%%%%%%%%%%%%%%%%%%%%%%%%%%%%%%%%
%
global dc dc_sim
% Diving the particles into small intervals by size (increment) to be able

```

```

% to sum all PSD for each Dp0 assuming that all particles in the interval have
the average size of that
% interval
%
increment=0.003;           % Size of the intervals (cm)
interval_size=0;          % Inicialization of the interval size variable
maximum=max(PSD_Dp_Save(:)); % Maximum particle size
number_intervals=round(maximum/increment)+1;
intervals=zeros(number_intervals,2);
%
for b=1:length(intervals)
    intervals(b,1)=intervals(b,1)+interval_size;
    interval_size=interval_size+increment;
end
%
for t=1:30000
    for a=1:length(dc_sim)
        for b=1:length(intervals)-1
            if intervals(b,1)<PSD_Dp_Save(t,a)
                if PSD_Dp_Save(t,a)<=intervals(b+1,1)

intervals(b,2)=intervals(b,2)+PSD_F_Dp_Save(t,a)*Fdp0_fraction(a);
                    end
                end
            end
        end
    end
end
%% Save of the PSD sum values
%
graph_x=zeros(1,length(intervals));
graph_y=zeros(1,length(intervals));
%
%
for c=1:1:length(intervals)
    if c==1
        graph_x(c)=increment/2*10000;
        graph_y(c)=intervals(c,2);
    else
        graph_x(c)=graph_x(c-1)+increment*10000;
        graph_y(c)=intervals(c,2);
    end
end
end
%

```